Biochimica et Biophysica Acta 1787 (2009) 995–1008

Contents lists available at ScienceDirect

Biochimica et Biophysica Acta

journal homepage: www.elsevier.com/locate/bbabio

Synthesis and characterization of *de novo* designed peptides modelling the binding sites of [4Fe–4S] clusters in photosystem I

Mikhail L. Antonkine [a,b,*], Melissa S. Koay [a], Boris Epel [a], Christoph Breitenstein [a], Oxana Gopta [c], Wolfgang Gärtner [a], Eckhard Bill [a], Wolfgang Lubitz [a,*]

[a] Max-Planck-Institut für Bioanorganische Chemie, Stiftstr. 34-36, D-45470 Mülheim an der Ruhr, Germany
[b] Fachbereich Physik, Institut für Experimental Physik (WE 1) Freie Universität Berlin, Arnimallee 14, D-14195 Berlin, Germany
[c] A.N. Belozersky Institute of Physico-Chemical Biology, Moscow State University, Vorob'evi Gori, 119899 Moscow, Russia

ARTICLE INFO

Article history:
Received 19 December 2008
Received in revised form 23 February 2009
Accepted 9 March 2009
Available online 16 March 2009

Keywords:
Model peptide
Iron–sulfur protein
[4Fe–4S] Cluster
PsaC
Photosystem I

ABSTRACT

Photosystem I (PS I) converts the energy of light into chemical energy *via* transmembrane charge separation. The terminal electron transfer cofactors in PS I are three low-potential [4Fe–4S] clusters named F_X, F_A and F_B, the last two are bound by the PsaC subunit. We have modelled the F_A and F_B binding sites by preparing two apo-peptides (maquettes), sixteen amino acids each. These model peptides incorporate the consensus [4Fe–4S] binding motif along with amino acids from the immediate environment of the iron–sulfur clusters F_A and F_B. The [4Fe–4S] clusters were successfully incorporated into these model peptides, as shown by optical absorbance, EPR and Mössbauer spectroscopies. The oxidation–reduction potential of the iron–sulfur cluster in the F_A-maquette is -0.44 ± 0.03 V and in the F_B-maquette is -0.47 ± 0.03 V. Both are close to that of F_A and F_B in PS I and are considerably more negative than that observed for other [4Fe–4S] model systems described earlier (Gibney, B. R., Mulholland, S. E., Rabanal, F., and Dutton, P. L. Proc. Natl. Acad. Sci. U.S.A. 93 (1996) 15041–15046). Our optical data show that both maquettes can irreversibly bind to PS I complexes, where PsaC-bound F_A and F_B were removed, and possibly participate in the light-induced electron transfer reaction in PS I.

1. Introduction

Iron–sulfur clusters are ubiquitous in biology and play many different roles in the living cell (reviewed in [1–5]). They act as catalysts, sensors and transcription regulators and play a signalling role during DNA repair. By far most common is their participation as redox cofactors in electron transfer reactions, either bound to a small soluble protein, as in ferredoxins, or as part of an electron transfer chain in a large protein or protein complex, as in hydrogenase or photosystem I. A wide variety of different iron–sulfur clusters exists in biology. The inventory of unique protein folds for different iron–sulfur proteins was recently compiled by Meyer [6].

Owing to their biological significance, iron–sulfur clusters have been extensively modelled in the past. A large body of literature exists on the investigation of chemically synthesized model compounds, mimicking iron–sulfur clusters of different nuclearity, in organic solvents (for a recent review see [7]). While providing valuable insight into the chemistry of the iron–sulfur clusters, the majority of these models cannot account for the interactions of the iron–sulfur cluster with its protein binding site, which includes interaction with non-ligating amino acids or with surrounding water molecules. Both types of interactions are believed to strongly influence the physiologically relevant properties of iron–sulfur clusters, *e.g.*, redox potential and catalytic activity.

In the past two decades several attempts were made to prepare models containing peptide or protein ligated iron–sulfur clusters in aqueous buffers [8–17]. Initially, the entire polypeptide sequence of ferredoxin from *Clostridium pasteurianum* [14,15], and a truncated polypeptide sequence from *Desulfovibrio gigas* ferredoxin II [16] were synthesized *in vitro*. More recently two main approaches for modelling binding sites were explored: the first relies on designing

Abbreviations: Chl *a*, Chlorophyll *a*; CW, Continuous Wave; DCPIP, 2,6-dichlorophenolindophenol; DIPEA, N,N-diisopropylethylamine; β-DM, n-dodecyl-β-D-maltoside; ENDOR, Electron Nuclear DOuble Resonance; EPR, Electron Paramagnetic Resonance; ESEEM, Electron Spin Echo Envelope Modulation; HYSCORE, HYperfine Sublevel COrRElation; HPLC, High Performance Liquid Chromatography; NADP, nicotinamide adenine nucleotide phosphate; NMP, N-methylpyrrolidone; MALDI-TOF-MS, Matrix Assisted Laser Desorption Ionisation – Time-of-Flight – Mass Spectrometry; P700-F_X core, PS I preparation where the stromal polypeptides PsaC, PsaD and PsaE, together with [4Fe–4S] clusters F_A and F_B, have been removed and the final electron acceptor is the [4Fe–4S] cluster F_X; P700-A_1 core, P700-F_X core where [4Fe–4S] cluster F_X have been removed and the final electron acceptor is the quinone A_1; PAL-PEG-PS, 5-(4-aminomethyl-3,5-dimethoxyphenoxy)valeryl polyethylene glycol-polystyrene; Pbf, 2,2,4,6,7-pentamethyldihydrobenzofuran-5-sulfonyl; PS I, Photosystem I; SHE, Standard Hydrogen Electrode; TCTU, O-(1H-6-Chlorobenzotriazole-1-yl)-1,1,3,3-tetramethyluronium tetrafluoroborate; PyBOP, benzotriazol-1-yl-oxytripyrrolidinophosphonium hexafluorophosphate; Trityl, Triphenylmethyl

* Corresponding authors. Tel.: +49 208 306 3892/3614; fax: +49 208 306 3951.
E-mail addresses: antonkin@mpi-muelheim.mpg.de (M.L. Antonkine), lubitz@mpi-muelheim.mpg.de (W. Lubitz).

0005-2728/$ – see front matter © 2009 Elsevier B.V. All rights reserved.
doi:10.1016/j.bbabio.2009.03.007

synthetic peptides containing the conserved iron–sulfur binding site [8–11]; the second relies on the introduction of the iron–sulfur cluster binding site into a naturally occurring or synthetic protein that was previously incapable of binding an iron–sulfur cluster [8,12,13,17]. It should be noted, however, that up to date only peptide-ligated models of [4Fe–4S] clusters were reported in the literature.

Incorporation of low-potential $[4Fe–4S]^{2+/1+}$ clusters into peptides of different sizes was investigated with the aim of determining the minimal requirements for successful binding [8–10]. Mulholland et al. investigated the influence of the amino acid composition of model peptides on the binding efficiency of iron–sulfur clusters [9,10]. In this study several model peptides with lengths between 4 and 16 amino acids were investigated. It was found that aside from the presence of a consensus iron–sulfur binding motif, containing at least three cysteines, which are appropriately spaced (CxxCxxC), the choice of non-liganding amino acids plays a decisive role in the efficiency of [4Fe–4S] cluster incorporation. By analysis of the amino acid sequence of 510 naturally occurring ferredoxins the prevalence of specific non-ligand amino acids in certain sequence positions within the consensus binding motif was established [10]. It was shown that β-branched amino acids like Ile or Val are dominant in the second position and Gly in the third and the fifth position. There seems to be less restriction for the choice of the sixth non-ligand amino acid in the consensus iron–sulfur cluster binding motif. While the apolar Ala is prevalent in this position (18%), a positively charged Arg is the second most prominent (12%) and Gln is also relatively common (8%).

Despite the variation of the amino acid composition, all previously studied maquettes containing a ferredoxin binding site show similar biophysical and biochemical properties, namely identical EPR spectra and a redox potential of about −0.350 V [8–10], or even higher, up to −0.289 V [11].

We consider that the next logical step is to model [4Fe–4S] cluster(s) which function within a large protein complex and whose biological role is well-known. Therefore, our attention turned to photosystem I (PS I), where the crystal structure of the overall complex is known [18], and the function of the [4Fe–4S] clusters in the electron transfer chain have been studied in detail for over 30 years and is well-established (see recent reviews collected in [19]).

PS I is a membrane-bound, multi-cofactor, energy-transforming protein complex, that is an indispensable part of the photosynthetic electron transfer chain in plants and cyanobacteria. PS I is a Type I reaction center, where the terminal electron acceptor is a [4Fe–4S] cluster. Three low-potential [4Fe–4S] clusters are bound on the reducing (stromal) side of PS I, usually referred as F_X, F_A and F_B (reviewed in [20]).

The [4Fe–4S] cluster F_X is an unusual case of an interpolypeptide iron–sulfur cluster, with two cysteine ligands provided by the PsaA subunit and two by the PsaB subunit of PS I. The binding site of F_X is identical on both subunits. Interestingly, F_X has one of the lowest midpoint reduction potentials known for a [4Fe–4S] cluster, values ranging from −0.730 V [21] to −0.705 V [22] (all potentials *versus* SHE). Scott et al. incorporated a binding motif of PS I [4Fe–4S] cluster F_X into the 4-α-helix bundle designed by the group of DeGrado [13]. This is the first, and so far the only model of both an iron–sulfur cluster involved in photosynthesis and of a interpolypeptide iron–sulfur cluster. It has an EPR spectrum nearly identical to maquettes containing the ferredoxin binding site, which is quite different from the EPR spectrum of the interpolypeptide [4Fe–4S] cluster F_X in PS I. This model, however, exhibits the lowest reduction potential found for a [4Fe–4S] cluster bound to a peptide maquette up to now (−0.422 V).

The iron–sulfur clusters, F_A and F_B, follow F_X in the electron transfer chain of PS I. They are bound to the PsaC subunit of PS I, which is located on the stromal side of the thylakoid membrane (Fig. 1A, for a recent review on PsaC structure and its binding to PS I see [23]). It was shown spectroscopically that F_B is the terminal electron acceptor in PS I [24–28] (reviewed in [20]). The midpoint reduction potentials of F_A and F_B in fully assembled PS I were measured at cryogenic

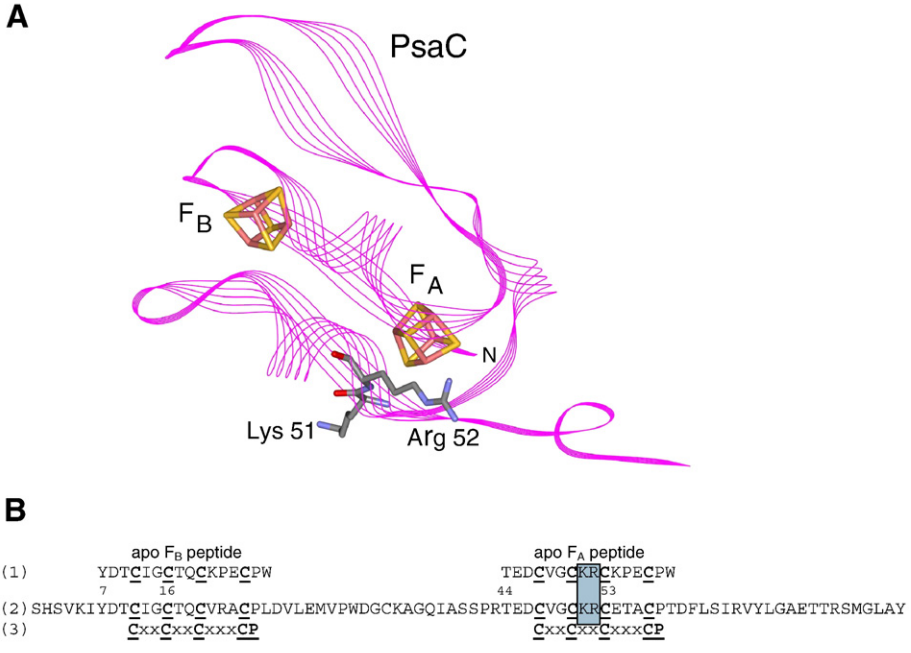

Fig. 1. (A) Three-dimensional structure of PsaC subunit taken from the X-ray structure of PS I at 2.5 Å resolution (PDB entry 1JB0) [18]. Detail of the structural model of the PS I monomer showing the backbone of the PsaC subunit and the [4Fe–4S] clusters F_A and F_B bound by it. The iron–sulfur clusters are shown as cubes, in which the yellow corners indicate position of sulfur atoms and light-brown corners the position of iron atoms. (B) Amino acid sequence of the designed peptides F_A and F_B (1) compared to the amino acid sequence of the PsaC subunit of PS I from *Synechococcus* sp. PCC 7002 (2) and the consensus low-potential [4Fe–4S] cluster binding motif (3). Numbering refers to the PsaC sequence. The Lys 51 and Arg 52 are crucial for binding of PsaC within PS I *via* the formation of salt bridges with amino acids on the PsaA and PsaB subunits [23,36]. They are shown as "stick" models in (A) and identified by the light blue box in (B).

temperature by redox titrations using EPR detection and were found to be −0.540 V and −0.590 V, respectively [29,30]. However, by titration of isolated PS I complexes using optical detection of the charge recombination between the iron–sulfur clusters and $P700^{\cdot+}$ at room temperature, potentials of −0.465 V and −0.440 V were found for F_A and F_B, respectively [31]. The latter potentials are closer to typical midpoint redox potentials found for [4Fe–4S] clusters in bacterial dicluster ferredoxins. It should be noted that in unbound PsaC F_A and F_B have a very similar midpoint reduction potential (ca. −0.460 V (J.H. Golbeck, personal communication)), which is different from the one in PS I-bound PsaC. It is impossible to obtain an independent reduction potential for either of the clusters in the unbound PsaC, most likely due to the fast exchange of an electron between the F_A and F_B clusters [32]. Note that PsaC experiences significant changes in its three-dimensional structure upon binding to the PS I core, especially in the presence of the PsaD subunit. These changes result in different EPR spectra of PS I-bound F_A and F_B and their altered reduction potentials [23,33–36]. Thus the spectroscopic and biochemical properties of the [4Fe–4S] clusters F_A and F_B are well-studied. The protein environment of both iron–sulfur clusters is also structurally well-characterized [18,35]. This makes F_A and F_B good targets for modelling. For an accurate comparison it would also be valuable to study in parallel [4Fe–4S] clusters bound to both the newly prepared model peptides and the PsaC subunit using the same techniques. Furthermore, we also want to test if our model peptides, with bound iron–sulfur clusters, could participate in the light-induced electron transfer. The availability of peptide models, that could be used as building blocks, is crucial for the construction of fully artificial or hybrid (chemical/biological) systems capable of photosynthetic charge separation.

2. Materials and methods

2.1. Synthesis of apo-F_A and apo-F_B peptides

Peptide synthesis was performed on an Advanced Chemtec 348Ω synthesizer. All chemicals were purchased from Iris Biotech and were used without further purification. PAL-PEG-PS resin was purchased from Applied Biosystems. The following side chain protection scheme for amino acids was applied: tert-butyl: Thr, Asp, Glu, Tyr; trityl: Gln, Cys; boc: Trp, Lys; Arg was protected by the Pbf group. Gly, Ile, Pro and Val were used without side chain protection. Amino acids and coupling reagents TCTU, PyBOP and DIPEA were dissolved in NMP. For deprotection a 25% solution of piperidine in DMF was used. During peptide synthesis, a ratio of 1:5:5:10 of resin:amino:acid:coupling: reagent:DIPEA was used. After each coupling and each deprotection the resin was washed six times with DMF. In a typical synthesis PAL-PEG-PS resin (258 mg, 0.17 mmol/g) was swollen two times in DMF for 30 min, followed by deprotection of the N-terminus (two times for 15 min each). For all amino acids double couplings were performed with a reaction time of 30 min per coupling step. After completion of the synthesis, the resin was washed four times with CH_2Cl_2, two times with methanol and again four times with CH_2Cl_2. The resin was dried for 90 min and the peptides were cleaved by a mixture of trifluoroacetic acid (36 ml), thioanisole (2.1 ml), ethanedithiol (1.2 ml) and anisol (0.9 ml). The resulting solution was stored over night at −20 °C to ensure complete deprotection. After removal of the cleavage solution under vacuum, the peptides were washed five times with diethyl ether/pentane 1:1, centrifuged, dissolved in water/acetic acid and freeze-dried.

Purification was done on a Vydac C18 Protein & Peptide column. A gradient over 45 min of acetonitrile and water was used starting at 20% and ending at 70% acetonitrile. All solvents contained 0.1% trifluoroacetic acid. The overall yield after purification (>99%) was 17% for both peptides F_A and F_B. Purity was proven by MALDI-TOF-MS for F_A (found 1850.5, calc.1852.8) and F_B (found 1845.6, calc. 1845.7).

2.2. Preparation of the C50G C33S variant of PsaC

The apo C50G C33S variant of the PsaC subunit of PS I was overproduced in *Escherichia coli* and purified as described previously [34].

2.3. Iron–sulfur cluster insertion

The [4Fe–4S] clusters were inserted into the apo-F_A and F_B peptides and apo C50G C33S PsaC by a previously described procedures [35,37–39], which is an adaptation of the original protocol of Lovenberg et al. [40]. Briefly, to 50 mM Tris/HCl, pH 8.3, 0.8% vol/vol 2-mercaptoethanol buffer a solution of 1 mg/ml apo peptide (or 5 mg/ml for apo PsaC) was added to a final peptide/protein concentration of 10 μM. This was followed by the dropwise addition of a 60 mM iron(III)chloride and a, freshly prepared, 60 mM sodium sulfide solutions to the final concentrations of 180 μM each. All additions were done in 20 minute intervals. All solutions and the Tris/HCl buffer were degassed and purged with argon prior to use. The reconstitution reaction was allowed to incubate overnight at 279 K. Then it was transferred to a Coy anaerobic chamber (COY Inc., Grass Lake, MI, USA) and all further manipulations were performed anaerobically. The iron–sulfur insertion reaction mixture was concentrated by ultrafiltration in an Amicon stirred cell (Millipore Corp.) furnished with a 1 kDa cut-off membrane (YM-1). Excess of unbound low molecular weight compounds was removed by passing the sample twice through a pre-packed gel-filtration column with Sephadex G-25 as solid phase (PD 10, GE Healthcare), where the dark brown fraction was collected. The sample was further concentrated by ultrafiltration as described above.

2.4. kPreparation of reduced samples of F_A and F_B peptides and the C13G C33S and C50G C33S variants of PsaC

Prior to reduction of iron–sulfur clusters, the pH of the samples was adjusted to 10.0 by addition of 1 M glycine buffer to a final concentration of 300 mM. Then a freshly prepared stock solution of 300 mM sodium dithionite was added to a final concentration of 30 mM. All manipulations were done inside the anaerobic chamber.

2.5. Preparation of ^{57}Fe enriched samples

$^{57}FeCl_3$ was prepared as follows: a known amount of solid ^{57}Fe was dissolved in concentrated HCl in electric contact to a sheet of platinum metal. After the reaction was complete (24–48 h), the solution was dried under vacuum. The yellow to red solid was dissolved in buffer inside the anaerobic chamber and the concentration of $^{57}FeCl_3$ was calculated from the initial amount of solid ^{57}Fe. $^{57}FeCl_3$ was used, in place of unlabeled iron (III) chloride, in iron–sulfur cluster insertion into the apo-F_A and F_B peptides and the apo C50G C33S PsaC variant using procedures described above.

2.6. Optical absorption spectroscopy

UV-Vis spectra were recorded on an ATI Unicam spectrometer model UV2-300, which was controlled by Thermo Spectronic software version 1.25. For all measurements gas-tight quartz cells with 1 cm path length were used. To determine the peptide concentration a calculated extinction coefficient of 5500 M^{-1} cm^{-1} for F_A and 6990 M^{-1} cm^{-1} for F_B was used [41]. The yield of iron-sulfur cluster incorporation was calculated using an extinction coefficient of $\varepsilon_{410} = 16{,}000$ M^{-1} cm^{-1} [42].

2.7. Continuous wave (CW) electron paramagnetic resonance (EPR) spectroscopy

CW EPR samples were measured on a Bruker E 500 spectrometer operating at X-band frequency. The temperature was controlled by an

Oxford ESR continuous flow cryostat model 910 combined with an Oxford ITC 503 intelligent temperature controller. The magnetic field was calibrated using a Bruker NMR Gaussmeter ER 035 M. Typical conditions for EPR measurements were: sample temperature 15 K, microwave frequency ca. 9.4 GHz, microwave power 20 mW, modulation frequency 100 kHz, modulation amplitude 10 G and time constant 40 ms, 5 scans. Simulations of holo F_A and holo F_B EPR spectra were performed using the EasySpin software [43,44], using the combination of Lorentzian and Gaussian linewidth broadening (pseudo-Voigt function) in order to represent natural linewidth and unresolved hyperfine structure of the EPR lines. In addition for better representation of the lineshapes anisotropic *g* strain was added.

2.8. Mössbauer spectroscopy

Mössbauer spectra were recorded on a spectrometer equipped with a Variox cryostat made by Oxford Instruments, and operating in the usual constant acceleration mode. The minimal experimental linewidth was 0.24 mm/s. The source was ^{57}Co in a 6 μm rhodium-matrix. Isomer shifts are referenced to α-iron at 300 K. All measured samples were enriched with ^{57}Fe.

2.9. Pulse EPR, ENDOR

2.9.1. Three pulse ESEEM measurements

Measurements were performed on the X-band Bruker Elexsys 580 spectrometer equipped with a dielectric cylindrical resonator. The temperature was controlled by an Oxford ITC liquid helium flow system. In all experiments the temperature was 10 K and the microwave frequency ca. 9.7 GHz. The length of all π/2 pulses was 16 ns. The delay time τ was 80 ns. The echo was integrated with a time window of 4 ns. The shot repetition rate was 1.5 ms. Prior to Fourier transformation the data were corrected using a polynomial base line. The cross-term averaging algorithm [45] was used to improve the phase stability of the Fourier transformed data.

2.9.2. Q-band ENDOR measurements

Measurements were performed using Q-band Bruker Elexsys 580 equipped with home-built cylindrical resonator [46,47]. The sample temperature was 6 K. A Davies ENDOR sequence with a 200 ns inversion pulse and a π/2–τ–π echo detection sequence (36 ns and 72 ns pulses, $\tau = 420$ ns) were used. A 15 μs radiofrequency pulse was applied. The repetition time was 5 ms.

2.10. Potentiometric titration of model peptides with bound iron–sulfur clusters

All potentiometric titrations were performed inside an anaerobic chamber. As a reference electrode, a home-built 1 M Ag/AgCl electrode (1 M KCl) was used, the working electrode was made of Pt wire. A calibrated high-impedance voltmeter was used to connect reference and working electrode (Radiometer, Copenhagen, Denmark). To rule out an error of the measured redox potential due to a hindered electrochemical contact between the solution and the electrode surface, the potentiometric titration of each peptide was repeated in the presence of mediators. However, the presence of the redox mediators such as indigo-tetrasulfonate (−0.046 V), phenosafranine (−0.252 V) and methyl viologen (−0.448 V) had no effect on the determined potential or on the overall titration.

2.10.1. UV-visible detection

The peptide solution was titrated with a solution of sodium dithionite in 1 M glycine buffer at pH 10. To the continuously stirred peptide solution an aliquot of 60 mM sodium dithionite was added and after a constant potential was reached, an aliquot was used to monitor the UV/Vis absorption. The titration was continued until an excess of sodium dithionite was visible at 315 nm in the UV/Vis spectra. This corresponds to a complete reduction of the sample. During the titration, aliquots were taken and several EPR samples were prepared and immediately frozen in liquid nitrogen to get an independent evidence of the reduction progress.

2.10.2. EPR detection

Prior to reductive titration, the reconstituted samples were adjusted to pH 10.0 using a stock solution of 1 M glycine buffer (pH 10.0). The final concentration of glycine was 300 mM. Sodium dithionite (300 mM $Na_2S_2O_4$ in 1 M glycine (pH 10.0)) was added in 1 μl aliquots to a continuously stirred solution of reconstituted peptide (~1.5 mM). The potential values were recorded after a steady potential reading was achieved. After each measurement, an aliquot of the peptide sample was removed and frozen in liquid nitrogen for EPR measurements.

The relative fraction of reduced [4Fe–4S] clusters was calculated based on the decrease of UV/Vis absorption at 410 nm or from the increase in amplitude of the EPR signal at g_3. Midpoint potentials were calculated by fitting the fraction of reduced [4Fe–4S] clusters *versus* the ambient potential of the solution to the Nernst equation for a one-electron transfer per oxidation/reduction process using a nonlinear Marquardt regression algorithm.

2.11. Time-resolved optical spectroscopy at 820 nm

The samples for kinetic measurements were prepared anaerobically in 50 mM Tris buffer (pH 8.3) containing 4 mM sodium ascorbate and 0.04% n-dodecyl-β-D-maltoside (β-DM) at Chl *a* concentrations of 70–100 μg/ml. Flash-induced absorbance changes were measured in the μs-to-s time range at 820 nm with a laboratory-built double-beam spectrometer as described previously [48]. The actinic flash was provided by a frequency-doubled, Nd-YAG laser ($\lambda = 532$ nm, 7 ns pulse duration, flash energy of ~2–3 mJ/cm^2, Quanta-Ray DCR-11, Spectra Physics, CA). Typically, 12 to 16 transients were recorded and averaged. Multiexponential fits of the kinetic data were performed using the PLUK software [49]. The best solution of the fitting was chosen based on the analysis of the residuals of the fits, the probability and correlation matrix for all fitted parameters.

2.12. Preparation of photosystem I, P700-F_X cores

The preparation of thylakoid membranes, the isolation of trimeric PS I complexes from *Synechococcus* sp. PCC 7002 using β-DM and the purification were done according to previously published procedures [50]. PS I complexes without F_A and F_B clusters (named P700-F_X cores) were isolated from PS I as described before [48]. Removal of the stromal subunits PsaD, PsaE, and PsaC with the terminal iron–sulfur clusters F_A and F_B, was followed by monitoring the kinetics of re-reduction of $P700^{\cdot+}$ at 820 nm. Independently, the removal of F_A and F_B clusters was verified by EPR spectroscopy (15 K, microwave frequency 9.436 GHz, microwave power 20 mW, modulation frequency 100 kHz, modulation amplitude 10 G). The sample was prepared by freezing of P700-F_X core in the presence of 10 mM of sodium ascorbate and 50 μM DCPIP under continuous illumination with a 150 W halogen lamp.

2.13. Rebinding of holo F_A and F_B peptides to P700-F_X core

For reconstruction of the P700-F_X core with the holo F_A or holo F_B peptide, P700-F_X core was incubated overnight in the dark on ice with a 10 times molar excess of the respective holo peptide. The non-bound peptide was then removed by repeated dilution-concentration on a Nanosep-100 concentrator with a 100 kDa molecular weight cut-off membrane (Pall Corp.). All manipulations were done inside an anaerobic chamber.

3. Results

3.1. Design of model peptides

The PsaC subunit of PS I is presumed to have evolved from bacterial ferredoxins which bind two [4Fe–4S] clusters (dicluster ferredoxins). However, the sequence similarity to them is restricted to having two [4Fe–4S] cluster binding motifs **C**(I)xx**C**(II)xx**C**(III)xxx**C**(IV)**P** and **C**(I′)xx**C**(II′)xx**C**(III′)xxx**C**(IV′)**P**. Cysteines I, II, III and IV′ ligate the first iron–sulfur cluster (F_B) and cysteines I′, II′, III′ and IV ligate the second iron–sulfur cluster (F_A) (reviewed in [23]) (Fig. 1). In our design approach these two ligation schemes are separated into two distinct peptides. The obvious point to dissociate the two binding sites is between cysteine IV and cysteine I′. In a second step the fourth ligand for each binding site needs to be relocated so that it lies in close vicinity to the first three cysteines. This can be achieved by introducing a short loop consisting of the residues KPE, where Pro is supposed to initiate the loop and the residues lysine and glutamate form a salt bridge to stabilize the preformed turn. This approach has been successfully used before [9]. Additionally, three preceding residues in front of the first cysteine have been introduced in order to provide additional shielding of the cluster and to avoid side reactions of the N-terminal cysteine residues during peptide synthesis. The peptide modelling the binding site of the F_B cluster of PsaC is named F_B peptide and the peptide modelling the binding site of the F_A cluster of PsaC is named F_A peptide. Except for the designed loop region, the native amino acid sequence of PsaC from *Synechococcus* sp. PCC 7002 has been used, *i.e.* Tyr 7 to Cys 16 for the sequence YDT**C**IG**C**TQ**C**KPE**C**PW (apo-F_B peptide); Thr 44 to Cys 53 for the sequence TED**C**VG**C**KR**C**KPE**C**PW (apo-F_A peptide) (Fig. 1B).

3.2. Peptide synthesis and iron–sulfur cluster insertion

The apo-F_A and apo-F_B were synthesized by the standard Fmoc-routine with an overall yield of 17% each. Neither a prolonged reaction time during amino acid coupling nor a change of coupling reagent had a significant effect on the yield. The relatively low yield during the synthesis may be due to the high abundance of Cys residues (four Cys out of 16-amino acids). Cysteine is known to undergo several side reactions during peptide synthesis [51]. The purity of the synthesized apo-peptides was controlled by analytical HPLC (>99%) and MALDI-TOF-MS (data not shown). The determined mass of each peptide corresponds to the calculated value within error: F_A peptide — found 1850.5 (calculated 1852.8), and F_B peptide — found 1845.6 (calculated 1845.7).

The extinction coefficient of both apo-peptides was estimated using the equation derived by Pace et al. [41]:

$$\varepsilon_{280}\left(M^{-1}\,\mathrm{cm}^{-1}\right) = 5500(\mathrm{Trp}) + 1490(\mathrm{Tyr}) \quad (1)$$

Here (Trp) and (Tyr) represent the number of the respective amino acid in the peptide sequence. In this manner, extinction coefficients of 5500 M^{-1} cm^{-1} and 6990 M^{-1} cm^{-1} were calculated for apo-F_A and apo-F_B, respectively.

Iron–sulfur clusters were inserted into the apo-F_A and F_B peptides as described in the Materials and methods section. The peptide is a chelate ligand, containing four cysteine residues, and it is expected to displace all the 2-mercaptoethanol molecules that initially ligate the [4Fe–4S] cluster formed in the reconstitution mixture. This was reported before for reconstitution of the PsaC subunit of PS I [35,37,38] and for insertion of iron–sulfur clusters into model peptides [8–10,13].

The reconstituted holo F_A and holo F_B peptides show a broad absorption in the visible range of the optical absorption spectrum with a maximum around 410 nm (Fig. 2). This is typical for oxidized iron–sulfur clusters and is ascribed to a sulfur to iron charge-transfer band. The extinction coefficient for a [4Fe–4S] cluster is about

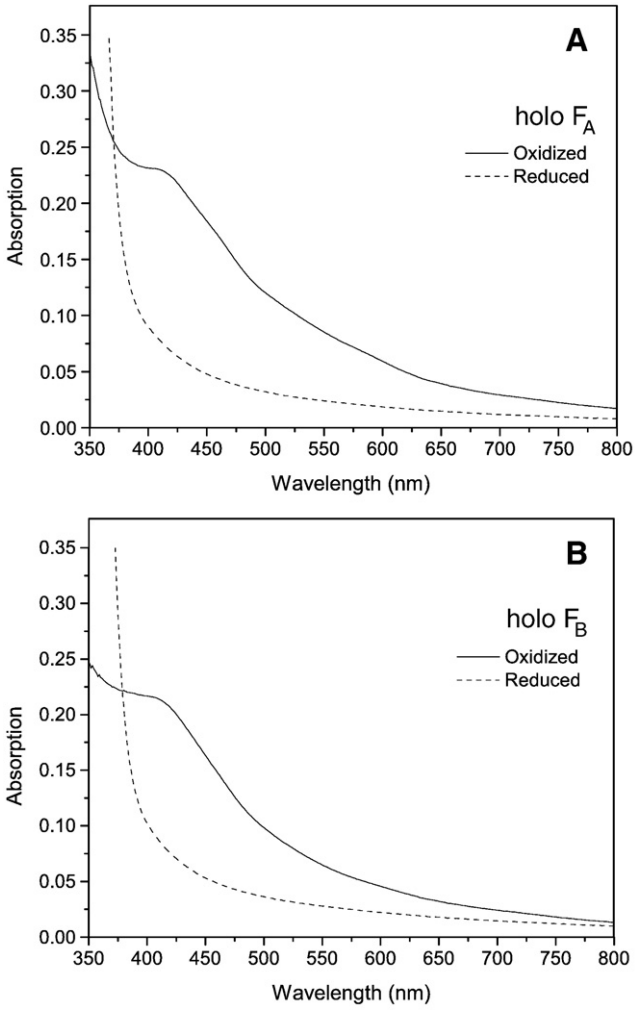

Fig. 2. Optical absorption spectrum of F_A (A) and F_B (B) peptides after insertion of the iron–sulfur clusters (holo peptides). The spectrum of the peptide with an oxidized iron–sulfur cluster is shown as solid line and the spectrum of the peptide with a reduced iron–sulfur cluster is shown as dashed line. Note that the loss of absorption around 410 nm upon reduction is typical for iron–sulfur clusters.

16,000 M^{-1} cm^{-1} at the absorption maximum [42]. The ratio of the concentrations calculated using the absorbances at 280 and 410 nm allows a calculation of the efficiency of iron–sulfur cluster reconstitution, which was found to be 24% for F_A and 12% for F_B.

The absorption at 410 nm is reduced significantly upon reduction of the sample by sodium dithionite, which is characteristic for iron–sulfur proteins. In summary, the UV/Vis spectra of the holo F_A and holo F_B peptides in the oxidized and reduced states (Fig. 2) are typical for protein/peptides binding iron–sulfur clusters.

3.3. Investigation of iron–sulfur clusters bound to model peptides by CW EPR spectroscopy

We used CW EPR spectroscopy at X-band to probe the identity of the iron–sulfur clusters bound to the holo F_A and holo F_B peptides.

A strong EPR spectrum was detected for the reduced holo F_A and holo F_B peptides (Fig. 3). In both cases it can only be simulated by assuming a rhombic *g*-tensor. The values, determined by simulation, are 2.04 (g_1), 1.93 (g_2), and 1.89 (g_3) for holo F_A; and 2.05 (g_1), 1.93 (g_2), and 1.90 (g_3) for holo F_B. EPR signals of iron–sulfur clusters bound to the holo F_A and holo F_B peptides cannot be observed above a temperature of 40 K due to excessive line broadening by fast spin relaxation [52]. The microwave power dependences of the EPR spectra observed for both the holo F_A and holo F_B peptides are

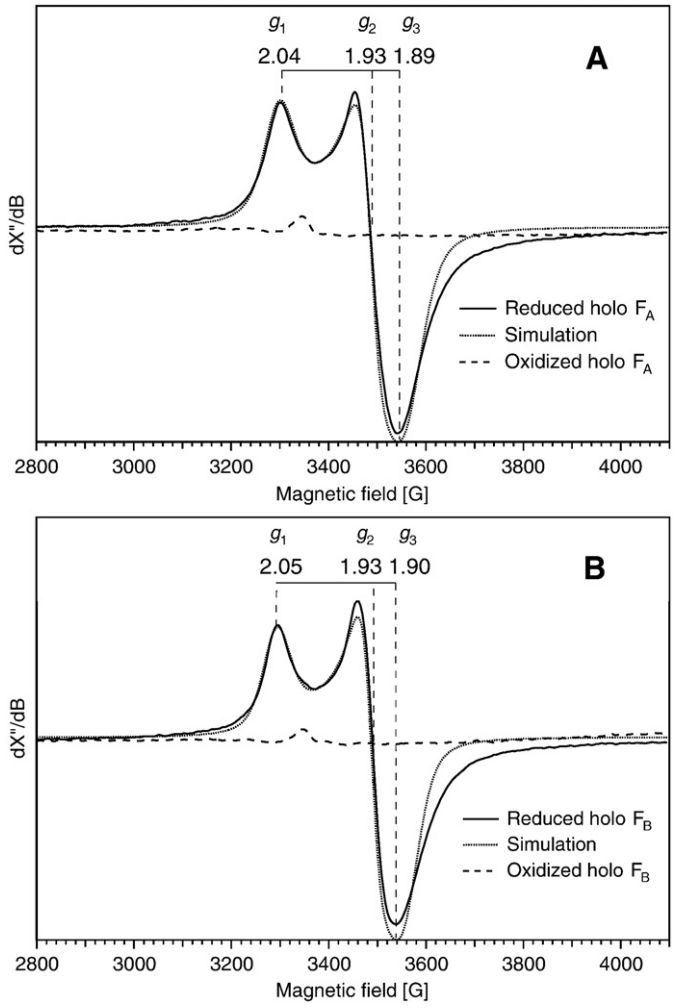

Fig. 3. EPR spectra of holo F_A peptide (A) and holo F_B peptide (B). Experimental traces of oxidized samples are shown by a dashed line; experimental traces of reduced samples are shown by a solid line, while their simulations are indicated by a dotted line. Experimental conditions: temperature 15 K, microwave frequency 9.436 GHz, microwave power 20 mW, modulation frequency 100 kHz, modulation amplitude 10 G. The principal components of *g*-tensors determined from the simulations are 2.04 (g_1), 1.93 (g_2) and 1.89 (g_3) for reduced holo F_A and 2.05 (g_1), 1.93 (g_2), and 1.90 (g_3) for reduced holo F_B. The precision of the *g*-tensor component determination is better than 0.005. The rhombicity of the *g*-tensors is evident from the simulations. Other simulation parameters for holo F_A: pseudo-Voigt lines with 50 G Lorentzian linewidth and 20 G Gaussian linewidth, *g* strain (0.03, 0.01, 0.03); for holo F_B: pseudo-Voigt lines with 40 G Lorentzian linewidth and 20 G Gaussian linewidth, *g* strain (0.03, 0.01, 0.03).

characteristic for the [4Fe–4S] cluster (not shown). The EPR signals of the iron–sulfur clusters can be maximized by variations of the microwave power and temperature. Highest signal intensities are obtained at 18 K and 200 mW for holo F_A and at 6 K and 200 mW for holo F_B. Thus EPR signals of both holo peptides could not be saturated under our experimental conditions using up to 200 mW of microwave power.

Similar EPR spectra were observed earlier for $[4Fe–4S]^{1+}$ clusters in single cluster ferredoxins, for model peptides [8–11] and also for PsaC (C13G C33S and C50G C33S mutants), where one of the iron–sulfur clusters is not detectable in the $g=2$ region of the EPR spectrum [53–55].

EPR signals characteristic for high-spin ($S\geq 3/2$) [4Fe–4S] clusters were not detected in reduced holo F_A and holo F_B in contrast to variants of PsaC described below [53–57].

Oxidized ($[4Fe–4S]^{2+}$) clusters are EPR silent due to strong antiferromagnetic coupling leading to a $S=0$ ground state. This is also found here for iron–sulfur clusters bound to holo F_A and holo F_B (see Fig. 3). Only a very weak signal of a [3Fe–4S] iron–sulfur cluster could be detected in the oxidized samples around $g\approx 2.01$ (Fig. 3) ($g_x=1.97$, $g_y=2.00$, and $g_z=2.02$) [39,52,58]. Since this signal has a much smaller linewidth than the reduced [4Fe–4S] cluster, the concentration of [3Fe–4S] clusters in our samples is very small. The formation of trace amounts of [3Fe–4S] clusters is common during *in vitro* iron–sulfur cluster reconstitution and was reported before [8,13,53].

3.4. Investigation of holo F_A and holo F_B peptides by Mössbauer spectroscopy

Zero-field Mössbauer spectra were recorded from ^{57}Fe-enriched samples of the holo F_A and holo F_B peptides at 80 K (Fig. 4) in order to identify the type and oxidation state of the iron–sulfur clusters (Fig. 4). The parameters obtained from data fits of the spectra with Lorentzian doublets are summarized in Table 1 for both the oxidized and reduced samples.

The Mössbauer sample of holo F_A in the oxidized state exhibits a dominating quadrupole doublet with an isomer shift, δ, of 0.43 mm/s and an electric quadrupole splitting, ΔE_Q, of 0.98 mm/s. Apparently the iron sites of the corresponding reconstituted iron–sulfur clusters are basically uniform and not distinguishable in the spectrum. The Mössbauer parameters for the corresponding contribution for oxidized holo F_B are $\delta=0.46$ mm/s and $\Delta E_Q=0.97$ mm/s. The moderate quadrupole splitting and particularly the intermediate values of the isomer shift for both peptides, holo F_A and holo F_B, are characteristic of tetrahedrally coordinated iron sites with four sulfur ligands and delocalized mixed valences of +2.5 [3,59,60].[1] This delocalized mixed-valence state is a unique feature of oxidized cubane [4Fe–4S] clusters in the 2+ state, which formally contain two Fe(II) and two Fe(III) ions. In contrast, other mixed-valence clusters like $[2Fe–2S]^{1+}$ and $[3Fe–4S]^{0}$ systems show distinguished iron sites due to (partial) valence localization.

The spectrum of oxidized holo F_B is slightly asymmetric, which we have to assign either to minor differences in the site symmetries or charge densities of the corresponding cluster, or to some heterogeneity of the protein preparation. Note that since EPR lines of reduced holo F_B are narrower than of holo F_A we find the latter one less likely. But like for holo F_A, individual contributions to the spectrum of holo F_B can also not be resolved within the experimental line width.

The sample of oxdized holo F_A shows a minor subspectrum (6% relative intensity) with isomer shift and quadrupole splitting of 1.3 mm/s and 3.00 mm/s in the sample. The very high isomer shift $\delta>1$ mm/s exceeds the range expected for iron–sulfur clusters and indicates iron(II) with hard oxo- or hydroxo-ligands. We, therefore, assign the subspectrum to adventitiously bound iron attached to the peptide. Similar species are also found in the spectra for both peptides in the reduced state.

Upon reduction the isomer shift and the quadrupole splitting of holo F_A increases by 0.08 mm/s and 0.05 mm/s, respectively. This trend again is typical of cubane iron–sulfur clusters for the reduction from the 2+ to the 1+ state (for a review see [59]). The values ($\delta=0.51$ mm/s, and $\Delta E_Q=1.03$ mm/s) resemble those of reduced ferredoxins [3,60].

To our surprise the zero-field Mössbauer spectrum of reduced holo F_B appears to have a single symmetric doublet with a similar change in the isomer shift, 0.06 mm/s as found for holo F_A, but with a reduced quadrupole splitting of 0.70 mm/s. Since we do not have further structural information we might only speculate why in this case the

[1] According to the empirical relation for the isomer shift of four-coordinated iron sulfur complexes [61], $\delta=1.4-0.4\,V$, where V is the valence of the iron sites. We obtain an average valence number of $V=+2.43$ for holo F_A and $V=+2.35$ for holo F_B.

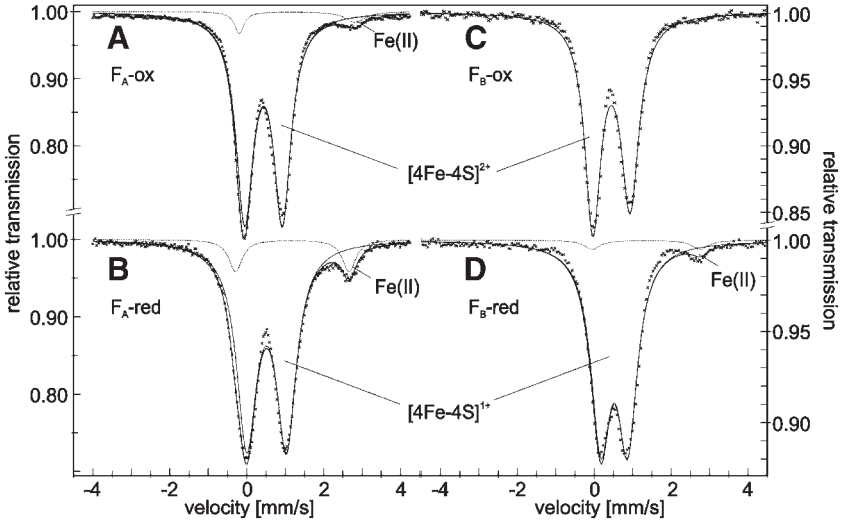

Fig. 4. Zero-field Mössbauer spectra of iron–sulfur clusters bound to F_A and F_B peptides as recorded at 80 K. Panels A and B show the spectra of an oxidized and a reduced holo F_A sample, panels C and D show the spectra of an oxidized and a reduced holo F_B. The experimental spectra (marks x) were simulated by using one or two Lorentzian doublets. The parameters for the major components, which we assign to the reconstituted [4Fe–4S] clusters, are summarized in Table 1. The minor doublets shown as dotted lines in A, B and D are due to iron(II) impurities, based on their parameters: (A) $\delta = 1.30$ mm/s, $\Delta E_Q = 3.00$ mm/s, linewidth = 0.30 mm/s, relative intensity 6%; (B) $\delta = 1.19$ mm/s, $\Delta E_Q = 2.95$ mm/s, linewidth = 0.42 mm/s, relative intensity 10%; and (D) $\delta = 1.35$ mm/s, $\Delta E_Q = 2.8$ mm/s, linewidth = 0.5 mm/s, relative intensity 4%.

reducing electron contributes an electric-field gradient with the opposite sign than for the other contributions to the efg.

In the C13G C33S variant the second cysteine ligand to the [4Fe–4S] cluster F_B (C13) is replaced by an external thiolate, and in the C50G C33S the second cysteine ligand to the [4Fe–4S] cluster F_A (C50) is replaced by an external thiolate [53,55]. The C13G C33S and C50G C33S variants of PsaC will later be used for comparison with holo F_A and holo F_B peptides, respectively (see Discussion). The C13G C33S variant of PsaC was studied earlier by Mössbauer spectroscopy [55] (Table 1). The C50G C33S variant of PsaC was investigated in this work and has an isomer shift of $\delta = 0.44$ mm/s and $\delta = 0.50$ mm/s in the oxidized and reduced state, respectively, upon reduction the quadrupole splitting increases from 0.88 mm/s to 0.97 mm/s (Table 1). The C13G C33S variant of PsaC in the reduced and oxidized states has an isomer shift identical to the C50G C33S variant, upon reduction the quadrupole splitting increases from 0.95 mm/s to 0.97 mm/s.

In summary, Mössbauer spectroscopy provides independent evidence that the [4Fe–4S] clusters are formed and that they are bound to the holo F_A and holo F_B peptides. The spectra can be clearly assigned for the oxidized samples containing diamagnetic ($[4Fe–4S]^{2+}$) clusters. The same interpretation should basically hold also for the reduced ($[4Fe–4S]^{1+}$) samples.

Table 1
Summary of Mössbauer parameters determined for iron–sulfur clusters bound to holo F_A and F_B determined at 80 K, as well as to C13G C33S and C50G C33S variants of the PsaC subunit of PS I.

Sample	δ [mm/s]	ΔE_Q [mm/s]	Linewidth [mm/s]
holo F_A peptide (oxidized)	0.43	0.98	0.54
holo F_A peptide (reduced)	0.51	1.03	0.63
C13G C33S PsaC (oxidized) [55]	0.44	0.95	0.44
C13G C33S PsaC (reduced) [55]	0.50	0.97	0.55
holo F_B peptide (oxidized)	0.46	0.97	0.50/0.56[a]
holo F_B peptide (reduced)	0.52	0.70	0.61
C50G C33S PsaC (oxidized)	0.44	0.88	0.58
C50G C33S PsaC (reduced)	0.50	0.97	0.55

Note that in the C13G variant the second cysteine ligand in the consensus binding site of the [4Fe–4S] cluster F_B is replaced by an external thiolate and in the C50G variant the second cysteine ligand in the consensus binding site of the [4Fe–4S] cluster F_A is replaced by an external thiolate [53,55].

[a] Widths of low-energy and high-energy lines.

3.5. Investigation of holo F_A and holo F_B peptides by pulse EPR, ESEEM and ENDOR spectroscopies

3.5.1. X-band ESEEM

Electron spin echo detected EPR spectra at X- and Q-band of both reduced holo F_A and holo F_B peptides as well as the C13G C33S variant of PsaC exhibited g-tensors identical to those found in the CW EPR study, see above and [55]. Fig. 5A shows the echo detected EPR spectrum of the holo F_B peptide as an example. The three-pulse ESEEM of the reduced holo F_A and holo F_B peptides, and the C13G C33S variant of PsaC were measured at the maxima of the corresponding EPR spectra, which is indicated by an arrow in Fig. 5A ($g_2 = 1.93$). Fig. 5B and C present the ESEEM spectra of holo F_A and holo F_B (solid lines). The higher frequency range of the ESEEM spectra was dominated by non-resolved ^{1}H couplings centered at the ^{1}H Larmor frequency of about 15 MHz (data not shown). In the low frequency range of the ESEEM spectra (0 to 5 MHz), multiple signals attributed to ^{14}N nuclei are observed. The ESEEM spectra of holo F_A and holo F_B peptides were simulated using a single set of parameters using the EasySpin software package [43,44]. The ^{14}N hyperfine coupling was assumed to be isotropic. The simulation results are presented in the corresponding figure together with the experimental data (Fig. 5B and C; dashed lines). For holo F_A we obtained an effective ^{14}N hyperfine coupling of 0.9 ± 0.05 MHz, a quadrupole coupling (e^2qQ/h) of 3.0 ± 0.1 MHz, and a quadrupole asymmetry parameter $\eta = 0.70 \pm 0.02$. For holo F_B the effective ^{14}N hyperfine coupling is 0.7 ± 0.07 MHz and the quadrupole coupling 3.1 ± 0.1 MHz, $\eta = 0.75 \pm 0.04$ (Table 2). Similar coupling were found in the ESEEM spectra of the C13G C33S variant of PsaC (data not shown).

The HYSCORE spectra [62] of the C13G C33S variant of PsaC and holo F_B were also recorded (data not shown). In the low frequency area those spectra showed a broad correlation ridge from (+3.1 MHz; +4 MHz) to (+4 MHz; +3.1 MHz) in the (+;+) quadrant, and an unresolved area in the (−;+) quadrant below (−2 MHz; +2 MHz). The position of the ridge confirmed our assignment of the ESEEM lines to an ^{14}N nucleus with a large quadrupole coupling. We did not observe additional correlation peaks that could be attributed to the same ^{14}N nucleus in the other quadrants. This could be due to anisotropy of the hyperfine coupling, which might result in a broad ridge. Due to the large error it was difficult to estimate the hyperfine anisotropy from the HYSCORE spectra and the isotropic hyperfine coupling had to be used for the ESEEM simulation. The signals in the area below (−2 MHz; +2 MHz)

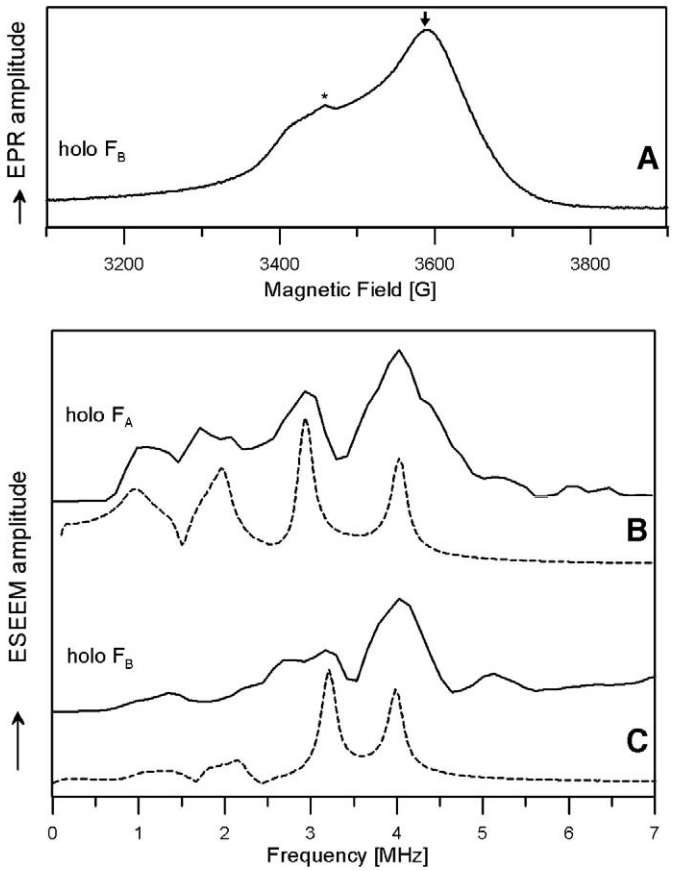

Fig. 5. (A) X-band pulse EPR spectrum of the reduced holo F_B peptide. The position of the maximum ($g_2 = 1.93$) of the EPR, where ESEEM was measured, is marked with an arrow. Note that the small signal at 3480 G (*) is due to excess of the sodium dithionite reductant. (B and C) The ESEEM spectra (solid lines) and simulations (dashed lines) of reduced holo F_A and holo F_B peptides. Simulation parameters for holo F_A peptide: $A_{iso} = 0.90 \pm 0.05$ MHz, $e^2qQ/h = 3.0 \pm 0.1$ MHz, $\eta = 0.70 \pm 0.02$ and for holo F_B peptide: $A_{iso} = 0.70 \pm 0.07$ MHz, $e^2qQ/h = 3.1 \pm 0.1$ MHz, $\eta = 0.75 \pm 0.04$.

most probably belong to several nuclei with small quadrupole couplings. Unfortunately, the low resolution of the spectra did not allow a more precise analysis of these signals. The signals, in the $(-;+)$ quadrant, cannot belong to the ^{14}N nucleus with the 3 MHz quadrupole coupling described above, according to our simulations.

The parameters obtained from the simulations of the holo F_A and holo F_B ESEEM spectra are very similar to those deduced from ESEEM spectra of several different iron–sulfur proteins [63–68]. Note that in these papers $[2Fe–2S]^+$ and $[3Fe–4S]^+$ clusters in proteins were studied. We are unaware of any previous ESEEM investigations of low-potential $[4Fe–4S]^+$ clusters in proteins or model peptides. Couplings, comparable in value to ours, were also determined from ENDOR spectra of iron–sulfur proteins (see for example [69,70]). Independently, similar ^{14}N quadrupole parameters were also observed in ESEEM spectra of model systems [71,72] and of other biological systems, for example in bacterial reaction center [73–75] (Table 2). In these works it was demonstrated that the size of the quadrupole coupling is indicative of a backbone amide that is hydrogen bonded to the spin-carrying center. In the iron–sulfur proteins such couplings were explained by the presence of hydrogen bonds between backbone amide protons (N–H) and the sulfur atoms of the cluster, which are typical for all iron–sulfur proteins. Both the bridging (μ-S) sulfurs of the cluster and/or the thiolate (S^-) sulfurs (mercaptides) of the cysteine ligands could be involved in such H-bonding of the iron–sulfur cluster.

Table 2
Selection of ^{14}N nuclear quadropole parameters of backbone nitrogens involved in hydrogen bonding to paramagnetic cofactors.

Protein/compound	e^2qQ/h, MHz	η	Reference
Di-glycine[a] N(2)	3.03	0.41	[71]
Tri-glycine[b] N(2)	3.01	0.48	[71]
Tri-glycine[b] N(3)	3.08	0.76	[71]
Polyglycine	3.097	0.76	[72]
Furmarate reductase Center 1 ($[2Fe–2S]^-$) from *Escherichia coli*	3.30	0.5	[65]
Bacterial reaction center ($Q_A^{\bullet -}$) from *Rhodopseudomonas viridis*	3.20	0.52	[73,74]
Bacterial reaction center ($Q_A^{\bullet -}$) from *Rhodobacter sphaeroides*	3.05	0.54	[73,75]
holo F_A peptide	3.0 ± 0.1	0.70 ± 0.02	This work
holo F_B peptide	3.1 ± 0.1	0.75 ± 0.04	This work

Comparison with holo F_A and holo F_B peptides.
[a] $^+H_3N(1)$-CH_2-CO-N(2)H-CH_2-COO^-.
[b] $^+H_3N(1)$-CH_2-CO-N(2)H-CH_2-CO-N(3)H-CH_2-COO^-.

3.5.2. Q-Band ENDOR

Two broad lines with maxima separated by approximately 1.9 MHz were observed in the ^1H ENDOR spectra of the reduced holo F_B peptide (Fig. 6). These lines were assigned to the β-CH_2 protons of cysteines ligating the [4Fe–4S] cluster. The eight β-CH_2 protons of all four cysteines ligating the [4Fe–4S] cluster most likely contribute to these lines [70,76,77]. Our assignment is based on the similarity to the previously described cases of β-CH_2 protons ligating the cubane [3Fe–4S] cluster in *D. gigas* hydrogenase [70], where a range of CH_2 hyperfine couplings of 1.3 to 1.9 MHz was found.

In a separate experiment the [4Fe–4S] clusters were inserted into the apo-F_B peptide in 99% deuterium oxide buffer (the pH was adjusted for the deuterium isotope effect). Since the apo peptide is completely unfolded and has no secondary structure in the absence of the iron–sulfur cluster, this should result in an exchange of all amide protons (H) to deuterons (D) prior to iron–sulfur cluster formation. In

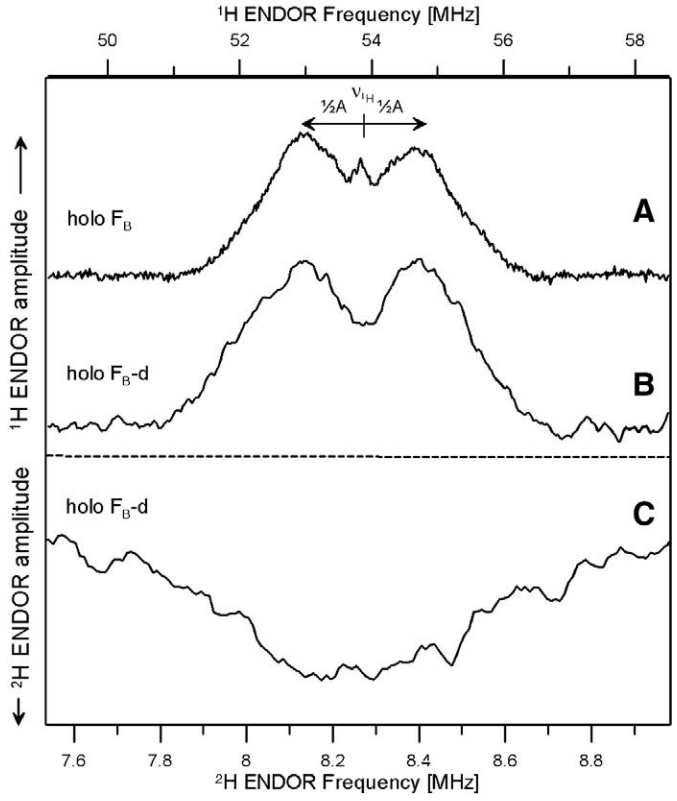

Fig. 6. (A) Q-band ^1H Davies ENDOR spectrum of the holo F_B peptide. (B) Q-band ^1H Davies ENDOR spectrum of the holo F_B peptide in 99.9% deuterated buffer. (C) ^2H Mims ENDOR spectrum of holo F_B peptide in deuterated buffer. All spectra were measured at the maximum of the EPR line ($g_2 = 1.93$) at 6 K.

the ^{1}H ENDOR spectra no effect on the lines with couplings larger than 1 MHz was detected upon deuteration (Fig. 6B). This corroborates our assignment of the strongly coupled lines to non-exchangeable β-CH_2 protons of cysteines ligating the [4Fe–4S] cluster. The amplitude of the signal at the ^{1}H Larmor frequency (matrix line) considerably decreased. The complementary deuterium ENDOR spectrum of the same holo F_B sample was also recorded (Fig. 6C). The ^{2}H ENDOR line is broad and unresolved. The width of the line (0.7 MHz) is significantly larger than that expected for matrix (bulk solvent) deuterons. This is due to the anisotropic hyperfine and quadrupole interactions [78,79]. Most likely the ^{2}H ENDOR line originates from the structural hydrogen bond(s) between the backbone ND group(s) and sulfur atom(s) of the [4Fe–4S] cluster. Hydrogen bonds between backbone nitrogens and the sulfur atoms of the iron–sulfur cluster are typical structural features of the ferredoxin binding sites in proteins [80]. This agrees well with the ESEEM data on the holo F_A and holo F_B peptides, discussed above. The EPR amplitude of the reduced holo F_A peptide at Q-band was found to be considerably smaller and insufficient for observation of the ^{1}H ENDOR spectra on this sample.

3.6. Oxidation–reduction potential of the [4Fe–4S] clusters bound to the F_A and F_B peptides

The redox potential of the holo F_A and the holo F_B peptides was determined by potentiometric titration (Fig. 7). Two different methods were used for detection of the gradual sample reduction during the titration. The first method relies on detection of the bleaching of the broad S→Fe charge-transfer band in the UV/Vis spectrum (around 400 nm) upon reduction of the iron–sulfur clusters. The second relies on EPR detection of the $[4Fe–4S]^{1+}$ $S=1/2$ signal, whose amount increases upon gradual reduction of the sample. In both cases, chemical reduction is performed by the addition of sodium dithionite at pH = 10 under strictly anaerobic conditions. Both methods give values identical within the error of the measurement. We estimated the redox potentials of holo F_A to be -0.44 ± 0.03 V and of holo F_B to be -0.47 ± 0.03 V.

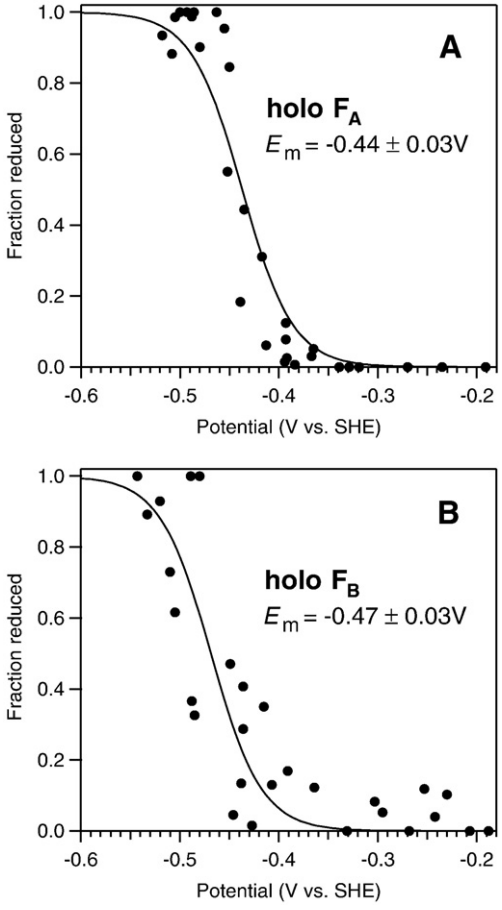

Fig. 7. Potentiometric titration of holo F_A (A) and holo F_B (B) peptides. The fraction of reduced [4Fe–4S] cluster has been plotted against the potential of the solution as measured against the standard hydrogen electrode. The amplitude of the $g_3 = 1.89$ EPR signal of the reduced [4Fe–4S] cluster (A) or UV/Vis absorption of the oxidized [4Fe–4S] cluster was used for detection (B). In (A) the normalized, combined data points of three separate titrations are used.

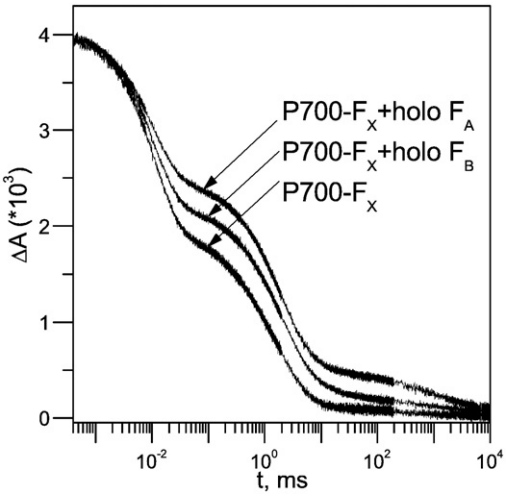

Fig. 8. Charge recombination kinetics of the $P700^{\cdot+}$ reduction, measured at 820 nm, in P700-F_X cores isolated from *Synechococcus* sp. PCC 7002 and their complexes with holo F_A or holo F_B peptides. Note, the appearance of longer lived kinetic phases indicating successful binding of the holo F_A or holo F_B model peptides to the P700-F_X core. See Table 3 for the analysis of kinetic phases.

3.7. Binding of the holo F_A and holo F_B peptides to the P700-F_x core

The P700-F_X core is a PS I preparation where the stromal subunits PsaC, PsaD and PsaE as well as the terminal [4Fe–4S] clusters F_A and F_B were removed by treatment of the PS I complex with chaotropic agents [81–83]. It is well-known that PsaC can be rebound to the P700-F_X core, re-establishing electron transfer to F_A/F_B [34,37,84,85] and the ability of PS I to reduce ferredoxin/flavodoxin upon a flash of light [56,86,87]. Since our peptides model the [4Fe–4S] clusters F_A and F_B of the PsaC subunit of PS I, we tested if each of them would be able to bind to the P700-F_X core and possibly participate in the light-induced electron transfer in PS I.

In isolated PS I, and complexes derived from it (such as the P700-F_X and other cores), photoinduced charge separation is followed by charge recombination between $P700^{\cdot+}$ and the terminal electron acceptor. This process could be monitored by measuring either the decay of the photoinduced absorbance change of the terminal acceptor, or the decay of the $P700^{\cdot+}$ after initiation of electron transfer by a laser flash. The latter approach has been used in this work both for monitoring the preparation of P700-F_X cores and for the investigation of the binding of the model peptides to these cores.

It was shown previously that the kinetics of backreaction in isolated PS I complexes is characterized by two main phases with lifetimes (τ) of ca. 30 and 100 ms [88,89] (reviewed in [90]). Note, that the backreaction lifetimes reported here are species and preparation dependent. In P700-F_X cores the terminal acceptors F_A and F_B are missing, consequently a faster reduction of $P700^{\cdot+}$ is observed with a backreaction occurring with τ of 10 and 200 μs, and 1.5–5 ms [48,85,91]. The P700-A_1 cores, isolated from PS I, additionally lack the interpolypeptide [4Fe–4S] cluster F_X [92]. Here the backreaction occurs with τ of ca. 10 and 200 μs and is attributed to charge recombination between $P700^{\cdot+}$ and $A_1^{\cdot-}$ [90,93,94]. In P700-F_X cores the

Table 3
Kinetic analysis of the $P700^{\cdot+}$ reduction measured at 820 nm in P700-F_X cores, isolated from *Synechococcus* sp. PCC 7002, and their complexes with holo F_A or holo F_B peptides.

Preparation	Backreaction lifetimes (τ) and their contributions (%)			
	$A_1^{\cdot-} \rightarrow P700^{\cdot+}$		$F_X^{\cdot-} \rightarrow P700^{\cdot+}$	New phases
	11 μs	260 μs	1.5–5 ms	>5 ms
P700-F_X cores	52%	8%	40%	–
P700-F_X cores complex with holo F_A	38%	4%	40%	18%
P700-F_X cores complex with holo F_B	46%	4%	40%	10%

backreactions in the μs time range are also attributed to charge recombination between $P700^{\cdot+}$ and $A_1^{\cdot-}$ and those in the ms time range to charge recombination between $P700^{\cdot+}$ and $F_X^{\cdot-}$ [85,90,93,94]. Gong et al. [85] showed that the contribution of the $P700^{\cdot+}$-$A_1^{\cdot-}$ charge recombination in part of the P700-F_X cores comes from the inhibition of electron transfer between A_1 and F_X in the absence of PsaC. Thus the presence of this phase in charge recombination is not due to the partial destruction of F_X during the isolation procedure and formation of some P700-A_1 cores instead of P700-F_X cores.

We isolated P700-F_X complexes from *Synechococcus* sp. PCC 7002 (see Materials and methods section). Either the holo F_A or holo F_B peptide was anaerobically incubated overnight with P700-F_X cores. The excess of peptide was removed by repeated ultrafiltration. Note that we attempted to individually bind the holo F_A or holo F_B peptides to P700-F_X cores. Charge recombination kinetics of the $P700^{\cdot+}$ reduction in the P700-F_X cores, and P700-F_X complexes with bound holo F_A or holo F_B peptides are shown in Fig. 8. Kinetic analysis of the $P700^{\cdot+}$ reduction in these preparations is summarized in Table 3.

Based on previous investigations of P700-F_X cores, the backreaction with lifetimes of 11 and 260 μs is attributed to recombination between $P700^{\cdot+}$ and $A_1^{\cdot-}$ and the backreaction with lifetimes 1.5–5 ms to charge recombination between $P700^{\cdot+}$ and $F_X^{\cdot-}$ [48,85,90,91,93,94]. The longer lived kinetic phases (>5 ms) were detected only in P700-F_X cores incubated with holo F_A or holo F_B peptides. Their appearance coincides with the decrease in the contribution of the kinetic phases belonging to the $P700^{\cdot+}$-$A_1^{\cdot-}$ charge recombination in P700-F_X core preparation.

Both peptides change the backreaction kinetics of P700-F_X cores irreversibly, since excessive washing does not recover the original backreaction kinetics (Materials and methods). Such changes in kinetics show that both holo F_A and holo F_B peptides can bind to P700-F_X cores and possibly participate in the light-induced electron transfer in PS I. An alternative explanation could be that our model peptides irreversibly change the environment of the interpolypeptide [4Fe–4S] cluster F_X leading to changes in the backreaction times. However, we believe that the latter explanation is rather unlikely.

The efficiency of holo F_A binding to P700-FX cores is higher (18%) than that of holo F_B (10%). This is not surprising since, unlike F_B, the F_A peptide sequence contains two key residues (Lys 51 and Arg 52) that are responsible for binding of PsaC to P700-F_X core [23,36] (Fig. 1).

In summary, according to our optical data both holo F_A and holo F_B irreversibly bind to P700-F_X cores and change the charge recombination kinetics.[2] This implies that they could participate in the light-induced electron transfer.

4. Discussion

4.1. Comparison of model peptides F_A and F_B with previous peptide-based models of [4Fe–4S] proteins

Two alternative modelling approaches were developed in the past few years to model [4Fe–4S] clusters in proteins. Gibney et al. showed that low-potential [4Fe–4S] clusters could be inserted into a sixteen amino acid synthetic polypeptide, whose sequence was derived from ferredoxin I from *Peptococcus aerogenes* [8]. Alternatively, a high-potential iron–sulfur cluster was successfully introduced into the hydrophobic core of thioredoxin from *E. coli* [12]. The former approach is close to the one we used in our work. Mulholland et al. focused on understanding the fundamental ligand requirements for the successful binding of low-potential [4Fe–4S] clusters by a sixteen amino acid maquettes [9]. In the follow-up work a minimal peptide, seven amino acids in length, which was capable of successful binding a low-potential [4Fe–4S] cluster was developed and the role of non-ligating amino acids in such maquettes was investigated [10].

The sequences of the synthetic peptides F_A and F_B, studied here satisfy the design rules established previously for model peptides [8–10]. Both peptides contain three appropriately spaced Cys residues, the second amino acid in the CxxCxxC motif is Val in F_A and Ile in F_B, the third position is occupied by Gly in both peptides. The fifth position is occupied by Lys in F_A and Thr in F_B. These two amino acids are the second and the third most prevalent at this position among previously studied iron–sulfur proteins [10]. An Arg residue that is found in F_A at the sixth position within the CxxCxxC binding motif is the second most prominent amino acid among all studied iron–sulfur proteins, while Gln found in F_B is also relatively common [10]. The fourth ligand to the iron–sulfur clusters is provided by Cys, which is part of the loop introduced by the KPECPW sequence, similarly to the ferredoxin maquette, FdM-Pa, described previously [9]. Note that in the binding site of F_A Lys at the fifth and Arg at the sixth positions are well conserved in PsaC sequences from diferent organisms since they play a key role in binding of PsaC to the P700-F_X core of PS I (Fig. 1A) [23,36].

The iron–sulfur cluster insertion procedure used here [35,37,38] is very similar to the one employed in previous studies of synthetic peptides modelling binding sites of [4Fe–4S] clusters [8–10], and is based on the original work of Lovenberg et al. [40]. Combination of the data obtained by optical, EPR and Mössbauer spectroscopies conclusively proves that low-potential [4Fe–4S] clusters are incorporated into both of our model peptides F_A and F_B (see Results and Figs. 2–4).[3]

4.2. Comparison of CW and pulse EPR and Mössbauer spectroscopic data obtained on holo F_A and holo F_B peptides and the PsaC subunit of PS I

This work focuses on the investigation of the properties of the [4Fe–4S] clusters bound to maquettes, which are compared to the properties of the [4Fe–4S] clusters bound to PsaC, investigated in parallel by identical methods. Wild-type PsaC contains two [4Fe–4S] clusters and, upon reduction, an "interaction spectrum" is observed reflecting magnetic interaction of two $S = 1/2$ paramagnetic centers. In order to circumvent this problem the EPR spectra of reduced holo F_A and holo F_B peptides were compared with the spectra measured on two variants of the PsaC in the reduced state.

[2] The detection of holo F_A and holo F_B bound to P700-F_X core by EPR at low temperature was attempted, but it was not successful. In these experiments PS I samples, typically of 0.5–0.6 mg/ml Chl concentration, are illuminated inside the EPR cavity (see [94] for a recent example) for accumulation of the $P700^{\cdot+}$-$F_A^{\cdot-}$ or $P700^{\cdot+}$+-$F_B^{\cdot-}$ states. In our case these experiments most likely did not succeed due to only partial binding of the model peptides to P700-F_X cores, which in both cases is under 20%. This leads to a low concentration of $P700^{\cdot+}$-holo $F_A^{\cdot-}$ or $P700^{\cdot+}$-holo $F_B^{\cdot-}$ states. Illumination of more concentrated sample is problematic due to the high optical density of the sample.

[3] The efficiency of iron–sulfur cluster reconstitution was found to be 24% for F_A and 12% for F_B. Note that the method used here for this calculation is very different from the one used before [8–10]. In the previous work, only the efficiency of iron–sulfur cluster reconstitution relative to the ferredoxin maquette (FdM) peptide was reported for synthetic peptides other than FdM [8–10]. For FdM it was reported to be > 60% based on spin-quantitation of the EPR signal of the dithionite-reduced [4Fe–4S] cluster [8], but unfortunately no details of this procedure were reported. Thus differences in procedure could account for discrepancies in the iron–sulfur cluster reconstitution efficiency of our and previously obtained data.

We use the C13G C33S and C50G C33S mutants of PsaC [53–55,86] for comparison to holo F_A and holo F_B peptides, respectively. The C13G C33S variant of PsaC lacks the second cysteine ligand in the binding site of the iron–sulfur cluster F_B (C13). Similarly, the C50G C33S variant of PsaC lacks the second cysteine ligand in the binding site of the iron–sulfur cluster F_A (C50). C33 in not involved in ligation of either F_A or F_B [4Fe–4S] clusters in PsaC, thus the C33S variant is used to reduce non-specific iron binding during insertion of the clusters [57]. Both C13G and C50G mutants are "rescued" by an external thiolate ligand which provides the fourth ligand to the iron–sulfur cluster. It is derived from 2-mercaptoethanol, which is present in the reaction mixture during iron–sulfur cluster reconstitution into the apo protein [53–55,86]. Interestingly, in the modified site the [4Fe–4S] cluster becomes $S \geq 3/2$ and appears to have no magnetic interaction with the second iron–sulfur cluster in the protein [55]. This allows the observation of the EPR signal, around $g = 2$, of the unmodified $S = 1/2$ iron–sulfur cluster F_A in the C13G C33S variant and F_B in the C50G C33S variant. The EPR signal of the mutated cluster is observed at g-values larger than 4.5 in both variants, $S \geq 3/2$ [53–55].

The EPR spectra, around $g = 2$, of both variants of PsaC are very similar with $g_1 = 2.04$, $g_2 = 1.93$ and $g_3 = 1.90$ for the F_A cluster (C13G C33S variant) and $g_1 = 2.05$, $g_2 = 1.93$ and $g_3 = 1.89$ for the F_B cluster (C50G C33S variant), the former one having a broader linewidth [53,55]). These values are nearly identical to those obtained for the reduced holo F_A and holo F_B peptides. Similarly, the reduced holo F_A peptide has a larger line width. These values are also very similar to the previously reported ones for model peptides binding iron–sulfur clusters, where $g_1 = 2.05$, $g_2 = 1.93$ and $g_3 = 1.89$ was found [8–11].

Previously, pulse EPR methods, such as ESEEM [95,96] and ENDOR [97,98], have been used successfully to investigate the local structure of paramagnetic centers in biological samples [99–102]. Up to now such methods have not yet been applied to peptide-based models of iron–sulfur clusters. ESEEM spectra recorded on the reduced holo F_A, holo F_B peptides (Fig. 5) and the C13G C33G variant of PsaC were consistent with structural hydrogen bond(s) between sulfur atom(s) and amide backbone proton(s) are present in the model peptides as well as in PsaC. The deuterium ENDOR spectrum obtained on reduced holo F_B peptide further supports this finding. Hydrogen bonding between backbone amide protons and sulfur atoms of the iron–sulfur cluster is a well-known structural feature of low-potential ferredoxins and shows that our peptides are realistic models for ferredoxins and for the PsaC subunit of PS I.

The Mössbauer spectra of the holo F_A and holo F_B peptides, both in the oxidized and reduced forms, were also compared to similar spectra of the C13G C33S and C50G C33S mutants of PsaC (Table 1). All the data indicate the presence of $[4Fe–4S]^{2+}$ clusters in the oxidized samples and $[4Fe–4S]^{1+}$ clusters in the reduced samples. Holo F_A and holo F_B peptides, to date, are only the second peptide-based models containing [4Fe–4S] clusters that were investigated by Mössbauer spectroscopy and the only ones investigated in both oxidized and reduced states. Previously helix–loop–helix peptides containing [4Fe–4S] and a bridged assembly [Ni^{2+}-(μ_2-S·Cys)-[4Fe–4S]] [17] were investigated by Mössbauer spectroscopy, confirming the presence of a [4Fe–4S] cluster in the oxidized (2+) state in both models.

4.3. Redox potentials of the model F_A and F_B peptides

Most of the previously designed models contained the Clostridial ferredoxin consensus iron–sulfur cluster binding site, including non-ligand amino acids [8,9,11]. These model peptides have a potential of −0.350 V [8,9] or even higher (−0.289 V) [11]. This lies within the broad range of potentials reported for low-potential iron–sulfur proteins in general [2]. However, these values are higher and different from the previously reported midpoint potentials of ferredoxins from *C. pasteurianum* (−0.403 V), *Clostridium acidi urici* (−0.434 V) and *P. aerogenes* (−0.427 V) [103,104]. The lowest redox potential, which is reported for a model peptide containing a $[4Fe–4S]^{2+/1+}$ cluster so far, is −0.422 V [13]. It was found for the 4-α-helix bundle containing the binding site of an interpolypeptide [4Fe–4S] cluster F_X of PS I [13]. Note, that the binding motif of F_X is drastically different from the Clostridial ferredoxin binding site.

Both model peptides described in our work contain the Clostridial ferredoxin consensus CxxCxxC [4Fe–4S] cluster binding motif. We determined the redox potential of holo F_A to be -0.44 ± 0.03 V and of holo F_B to be -0.47 ± 0.03 V. Note that our data are an upper estimate and the actual potential could be even lower. Also, while the error of our measurement is quite significant the potentials that we found are at least 0.05 to 0.09 V more negative than those previously published for short peptides modelling Clostridial ferredoxins [8,9] and are very close to the data obtained for the only reported model for the [4Fe–4S] cluster F_X [13]. More importantly, these potentials are very close to typical midpoint redox potentials found for [4Fe–4S] clusters in bacterial ferredoxins. They correlate well with the redox potentials of −0.465 V and −0.440 V that were found for F_A and F_B, respectively, in PS I [31]. This underlines the biological relevance of our models.

In the ESEEM and ^2H ENDOR spectra (Figs. 5 and 6) we detected hydrogen bond(s) between sulfur atom(s) of the cluster and the backbone amide proton(s). This is known to stabilize the reduced (1+) state of [4Fe–4S] clusters [80,104] which lowers the reduction potential. Solvent accessibility is another feature that contributes to the decrease of the reduction potential of [4Fe–4S] clusters [80,104]. The broadness of the ENDOR line belonging to β-CH_2 protons of cysteines ligating the [4Fe–4S] cluster in the holo F_B peptide indicates flexibility of the polypeptide chain around the metal center, thus allowing virtually unhindered, *i.e.* easy access of water molecules to the cluster.

4.4. Binding of the holo F_A and holo F_B models to P700-F_X cores

After successful modelling of the iron–sulfur clusters F_A and F_B bound to the PS I subunit PsaC, it is important to determine if each of our models can bind to PS I (P700-F_X core) and possibly participate in the light-initiated electron transfer in PS I. This would open a way for practical use of these models as building blocks in the construction of biomimetic systems that can be used for energy production.

As described above, the F_A peptide sequence contains two key residues (Lys 51 and Arg 52, Fig. 1) that are crucial for binding of PsaC to the P700-F_X core *via* the formation of salt bridges with amino acids on the PsaA and PsaB subunits [23,36]. In contrast, the F_B peptide does not contain such residues. Therefore, it is quite surprising that holo F_B is capable of binding to the PS I cores at all. However, as expected, binding of holo F_A is more efficient (18% for holo F_A and 10% for holo F_B). It is interesting to compare our data with rebinding of PsaC to P700-F_X cores *in vitro*.

The PsaC deletion mutant was constructed in *Synechocystis* sp. PCC 6803 [85,105], rendering cells that were incapable of photoautotrophic growth. PS I is assembled in this mutant. However, it lacks the stromal subunits PsaC, PsaD and PsaE as well as the PsaC-bound terminal [4Fe–4S] clusters F_A and F_B. Thus, the *in vivo* P700-F_X core is formed, which could be isolated from these cells without chemical treatment of the PS I complex. It was shown that recombinant PsaC could be rebound to these P700-F_X cores [56,85]. However, a reduced efficiency of rebinding was reported: 43% [56] and 32% [85]. The rebinding of recombinant PsaC to P700-F_X cores, prepared by urea treatment of PS I, was reported to occur with 41% efficiency [86]. In summary, the results obtained on rebinding PsaC *in vitro* are compatible to our results on binding of the small peptides holo F_A (18%) and holo F_B (10%) to P700-F_X cores.

Binding of holo F_A and holo F_B to P700-F_X cores isolated from two different cyanobacterial species *Synechocystis* sp. PCC 6803 (data not shown) and *Synechococcus* sp. PCC 7002 implies that such binding is a general quality rather than a species specific effect.

An important point is that our evidence for binding of holo F_A and holo F_B to P700-F_X cores are based solely on the irreversible change of the charge recombination in P700-F_X cores upon incubation with either holo F_A or holo F_B peptides. We are continuing our research and are looking for further evidence of this.

Overall, it is quite exciting that the small peptides can bind to PS I cores and participate in the light-induced electron transfer. This can be used for chemical attachment of different molecules to the acceptor side of PS I. It could be done, for example, *via* attaching a chemical rescue ligand to the [4Fe–4S] cluster, as described previously [55], and/or by directly engineering proper amino acids in the binding sequence of the custom designed peptides. These findings could have implications for the construction of new alternative energy sources, *e.g.* for light-driven hydrogen production, specifically, if similar peptide models will be used to attach [FeFe] or [NiFe] hydrogenases directly to PS I [106].

5. Summary and conclusions

Two sixteen amino acid peptides modelling the binding sites of the [4Fe–4S] clusters F_A and F_B of photosystem I were prepared. By optical-, EPR- and Mössbauer spectroscopies it has been conclusively proven that holo F_A and holo F_B model peptides bind $[4Fe–4S]^{2+/1+}$ clusters. The midpoint reduction potential of holo F_A was determined to be -0.44 ± 0.03 V and that of holo F_B to be -0.47 ± 0.03 V. These values are considerably lower than the ones previously reported for similar model systems and are very close to the ones of F_A and F_B in photosystem I. By ESEEM and ^{2}H ENDOR spectroscopies it was shown that the iron–sulfur clusters in both peptides are hydrogen bonded *via* amide of the peptide backbone. This demonstrates the structural integrity of our models and could, in part, explain the relatively low reduction potential found for holo F_A and holo F_B. By optical spectroscopy we have found that both model peptides can bind to the P700-F_X core. Our data suggest that bound peptides could serve as electron acceptors during light-initiated electron transfer. The ability of the model peptides to participate in the light-induced electron transfer can open new avenues for the construction of hybrid biological/chemical systems for conversion of light into chemical energy.

Acknowledgements

This work is dedicated to the memory of Peter Paul Schmidt (1960-2008). Technical help of Irina Michin, Robert Dickmann and Ingeborg Heise is gratefully acknowledged. We thank John H. Golbeck from The Pennsylvania State University for the possibility to prepare apo C50G C33S PsaC and P700-F_X cores as well as for the use of his optical spectroscopy setup for measuring the backreaction kinetics. We are grateful to Eberhard Schlodder from the Technical University of Berlin for the possibility to perform additional optical measurements, preceded and followed by stimulating and fruitful discussions of binding of peptides to P700-F_X cores. The Max Planck Society is acknowledged for generous funding of this work. Additional funding was provided by DFG (Sfb 498, TP A3) to M.L.A.

References

[1] M. Fontecave, Iron–sulfur clusters: ever-expanding roles, Nat. Chem. Biol. 2 (2006) 171–174.
[2] H. Beinert, Iron–sulfur proteins: ancient structures, still full of surprises, J. Biol. Inorg. Chem. 5 (2000) 2–15.
[3] H. Beinert, R.H. Holm, E. Münck, Iron–sulfur clusters: nature's modular, multipurpose structures, Science 277 (1997) 653–659.
[4] H. Beinert, P.J. Kiley, Fe–S proteins in sensing and regulatory functions, Curr. Opin. Chem. Biol. 3 (1999) 152–157.
[5] P.J. Kiley, H. Beinert, The role of Fe–S proteins in sensing and regulation in bacteria, Curr. Opin. Microbiol. 6 (2003) 181–185.
[6] J. Meyer, Iron–sulfur protein folds, iron–sulfur chemistry, and evolution, J. Biol. Inorg. Chem. 13 (2008) 157–170.
[7] P.V. Rao, R.H. Holm, Synthetic analogues of the active sites of iron–sulfur proteins, Chem. Rev. 104 (2004) 527–559.
[8] B.R. Gibney, S.E. Mulholland, F. Rabanal, P.L. Dutton, Ferredoxin and ferredoxin-heme maquettes, Proc. Natl. Acad. Sci. U. S. A. 93 (1996) 15041–15046.
[9] S.E. Mulholland, B.R. Gibney, F. Rabanal, P.L. Dutton, Characterization of the fundamental protein ligand requirements of [4Fe–4S](2+/+) clusters with sixteen amino acid maquettes, J. Am. Chem. Soc. 120 (1998) 10296–10302.
[10] S.E. Mulholland, B.R. Gibney, F. Rabanal, P.L. Dutton, Determination of nonligand amino acids critical to 4Fe–4S (2+/+) assembly in ferredoxin maquettes, Biochemistry 38 (1999) 10442–10448.
[11] M.L. Kennedy, B.R. Gibney, Proton coupling to 4Fe–4S (2+/+) and 4Fe–4Se (2+/+) oxidation and reduction in a designed protein, J. Am. Chem. Soc. 124 (2002) 6826–6827.
[12] C.D. Coldren, H.W. Hellinga, J.P. Caradonna, The rational design and construction of a cuboidal iron–sulfur protein, Proc. Natl. Acad. Sci. U. S. A. 94 (1997) 6635–6640.
[13] M.P. Scott, J. Biggins, Introduction of a [4Fe–4S (S-cys)4](+1,+2) iron–sulfur center into a four-alpha helix protein using design parameters from the domain of the F-x cluster in the Photosystem I reaction center, Protein Sci. 6 (1997) 340–346.
[14] E. Smith, J. Tomich, T. Iwamoto, J. Richards, Y. Mao, B. Feinberg, A totally synthetic histidine-2 ferredoxin — thermal stability and redox properties, Biochemistry 30 (1991) 11669–11676.
[15] E.T. Smith, B.A. Feinberg, J.H. Richards, J.M. Tomich, Physical characterization of a totally synthetic 2 4Fe–4S Clostridial ferredoxin, J. Am. Chem. Soc. 113 (1991) 688–689.
[16] T.C. Sow, M.V. Pedersen, H.E.M. Christensen, B.L. Ooi, Total synthesis of a miniferredoxin, Biochem. Biophys. Res. Commun. 223 (1996) 360–364.
[17] C.E. Laplaza, R.H. Holm, Helix–loop–helix peptides as scaffolds for the construction of bridged metal assemblies in proteins: the spectroscopic A-cluster structure in carbon monoxide dehydrogenase, J. Am. Chem. Soc. 123 (2001) 10255–10264.
[18] P. Jordan, P. Fromme, H.T. Witt, O. Klukas, W. Saenger, N. Krauss, Three-dimensional structure of cyanobacterial photosystem I at 2.5 Å resolution, Nature 411 (2001) 909–917.
[19] J.H. Golbeck, Photosystem I. The light-driven plastocyanin:ferredoxin oxidoreductase, Advances in Photosynthesis and Respiration Govindjee, Springer, The Netherlands, 2006.
[20] I.R. Vassiliev, M.L. Antonkine, J.H. Golbeck, Iron–sulfur clusters in type I reaction centers, Biochim. Biophys. Acta, Bioenerg. 1507 (2001) 139–160.
[21] B. Ke, E. Dolan, K. Sugahara, F.M. Hawkridge, S. Demeter, E.R. Shaw, Electrochemical and kinetic evidence for a transient electron acceptor in the photochemical charge separation in photosystem I, Plant Cell Physiol. (1977) 187–199.
[22] S.K. Chamorovsky, R. Cammack, Direct determination of the midpoint potential of the acceptor X in chloroplast photosystem I by electrochemical reduction and ESR spectroscopy, Photobiochem. Photobiophys. 4 (1982) 195–200.
[23] M.L. Antonkine, J.H. Golbeck, Molecular interactions of the stromal subunit PsaC with PsaA/PsaB heterodimer, in: J.H. Golbeck (Ed.), Photosystem I. The Light-Driven Plastocyanin:Ferredoxin Oxidoreductase, Springer, The Netherlands, 2006, pp. 79–98.
[24] A. Diaz-Quintana, W. Leibl, H. Bottin, P. Setif, Electron transfer in photosystem I reaction centers follows a linear pathway in which iron–sulfur cluster F_B is the immediate electron donor to soluble ferredoxin, Biochemistry 37 (1998) 3429–3439.
[25] Y.S. Jung, L. Yu, J.H. Golbeck, Reconstitution of iron–sulfur center F_B results in complete restoration of $NADP^{(+)}$ photoreduction in Hg-treated Photosystem I complexes from *Synechococcus* sp PCC 6301, Photosynth. Res. 46 (1995) 249–255.
[26] I.R. Vassiliev, Y.S. Jung, F. Yang, J.H. Golbeck, PsaC subunit of photosystem I is oriented with iron–sulfur cluster F-B as the immediate electron donor to ferredoxin and flavodoxin, Biophys. J. 74 (1998) 2029–2035.
[27] K.V. Lakshmi, Y.S. Jung, J.H. Golbeck, G.W. Brudvig, Location of the iron–sulfur clusters F_A and F_B in photosystem I: an electron paramagnetic resonance study of spin relaxation enhancement of $P700^+$, Biochemistry 38 (1999) 13210–13215.
[28] V.P. Shinkarev, I.R. Vassiliev, J.H. Golbeck, A kinetic assessment of the sequence of electron transfer from F(X) to F(A) and further to F(B) in photosystem I: the value of the equilibrium constant between F(X) and F(A), Biophys. J. 78 (2000) 363–372.
[29] M.C.W. Evans, S.G. Reeves, R. Cammack, Determination of the oxidation–reduction potential of the bound iron–sulfur proteins of the primary electron acceptor complex of photosystem I in spinach chloroplasts, FEBS Lett. 49 (1974) 111–114.
[30] M.C.W. Evans, P. Heathcote, Effects of glycerol on the redox properties of the electron acceptor complex in spinach photosystem I particles, Biochim. Biophys. Acta 590 (1980) 89–96.
[31] R. Jordan, U. Nessau, E. Schlodder, Charge recombination between the reduced iron–sulfur clusters and $P700^+$, in: G. Garab (Ed.), Photosynthesis: Mechanisms and Effects, Kluwer Acad. Publ., Dordrecht, 1998, pp. 663–666.
[32] D. Bentrop, I. Bertini, C. Luchinat, W. Nitschke, U. Mühlenhoff, Characterization of the unbound 2[Fe4S4]-ferredoxin-like photosystem I subunit PsaC from the cyanobacterium *Synechococcus elongatus*, Biochemistry 36 (1997) 13629–13637.
[33] N. Li, J. Zhao, P.V. Warren, J.T. Warden, D.A. Bryant, J.H. Golbeck, PsaD is required for the stable binding of PsaC to the photosystem I core protein of *Synechococcus* sp. PCC 6301, Biochemistry 30 (1991) 7863–7872.
[34] J. Zhao, P.V. Warren, N. Li, D.A. Bryant, J.H. Golbeck, Reconstitution of electron transport in photosystem I with PsaC and PsaD proteins expressed in *Escherichia coli*, FEBS Lett. 276 (1990) 175–180.

[35] M.L. Antonkine, G.H. Liu, D. Bentrop, D.A. Bryant, I. Bertini, C. Luchinat, J.H. Golbeck, D. Stehlik, Solution structure of the unbound, oxidized photosystem I subunit PsaC, containing 4Fe–4S clusters F_A and F_B: a conformational change occurs upon binding to photosystem I, J. Biol. Inorg. Chem. 7 (2002) 461–472.

[36] M.L. Antonkine, P. Jordan, P. Fromme, N. Krauss, J.H. Golbeck, D. Stehlik, Assembly of protein subunits within the stromal ridge of photosystem I. Structural changes between unbound and sequentially PS I-bound polypeptides and correlated changes of the magnetic properties of the terminal iron sulfur clusters, J. Mol. Biol. 327 (2003) 671–697.

[37] T. Mehari, K.G. Parrett, P.V. Warren, J.H. Golbeck, Reconstitution of the iron–sulfur clusters in the isolated FA/FB protein: EPR spectral characterization of same-species and cross-species photosystem I complexes, Biochim. Biophys. Acta 1056 (1991) 139–148.

[38] M.L. Antonkine, D. Bentrop, I. Bertini, C. Luchinat, G. Shen, D.A. Bryant, D. Stehlik, J.H. Golbeck, Paramagnetic ^{1}H NMR spectroscopy of the reduced, unbound photosystem I subunit PsaC: sequence-specific assignment of contact-shifted resonances and identification of mixed- and equal-valence Fe–Fe pairs in [4Fe–4S] centers F_A^- and F_B^-, J. Biol. Inorg. Chem. 5 (2000) 381–392.

[39] U. Leartsakulpanich, M.L. Antonkine, J.G. Ferry, Site-specific mutational analysis of a novel cysteine motif proposed to ligate the 4Fe–4S cluster in the iron–sulfur flavoprotein of the thermophilic methanoarchaeon *Methanosarcina thermophila*, J. Bacteriol. 182 (2000) 5309–5316.

[40] W. Lovenberg, J.C. Rabinowitz, B.B. Buchanan, Studies on chemical nature of Clostridial ferredoxin, J. Biol. Chem. 238 (1963) 3899–3913.

[41] C.N. Pace, F. Vajdos, L. Fee, G. Grimsley, T. Gray, How to measure and predict the molar absorption-coefficient of a protein, Protein Sci. 4 (1995) 2411–2423.

[42] W.V. Sweeney, J.C. Rabinowitz, Proteins containing 4Fe–4S clusters — an overview, Ann. Rev. Biochem. 49 (1980) 139–161.

[43] S. Stoll, A. Schweiger, EasySpin, a comprehensive software package for spectral simulation and analysis in EPR, J. Magn. Res. 178 (2006) 42–55.

[44] S. Stoll, A. Schweiger, EasySpin: simulating cw ESR spectra, Biol. Magn. Reson. 27 (2007) 299–321.

[45] A. Schweiger, G. Jeschke, Principles of Pulse Electron Paramagnetic Resonance, Oxford University Press, New York, 2001.

[46] S. Sinnecker, E. Reijerse, F. Neese, W. Lubitz, Hydrogen bond geometries from electron paramagnetic resonance and electron-nuclear double resonance parameters: density functional study of quinone radical anion-solvent interactions, J. Am. Chem. Soc. 126 (2004) 3280–3290.

[47] A. Silakov, E.J. Reijerse, S.P.J. Albracht, E.C. Hatchikian, W. Lubitz, The electronic structure of the H-cluster in the FeFe-hydrogenase from *Desulfovibrio desulfuricans:* a Q-band Fe-57-ENDOR and HYSCORE study, J. Am. Chem. Soc. 129 (2007) 11447–11458.

[48] I.R. Vassiliev, Y.S. Jung, L.B. Smart, R. Schulz, L. Mcintosh, J.H. Golbeck, A mixed-ligand iron–sulfur cluster (C556S(PsaB) or C565S(PsaB)) in the F-x-binding site leads to a decreased quantum efficiency of electron transfer in photosystem, Biophys. J. 69 (1995) 1544–1553.

[49] Y.L. Kalaidzidis, A.V. Gavrilov, P.V. Zaitsev, A.L. Kalaidzidis, E.V. Korolev, PLUK — An environment for software development, Program. Comput. Softw. 23 (1997) 206–211.

[50] G.Z. Shen, J.D. Zhao, S.K. Reimer, M.L. Antonkine, Q. Cai, S.M. Weiland, J.H. Golbeck, D.A. Bryant, Assembly of photosystem I: I. Inactivation of the *rubA* gene encoding a membrane-associated rubredoxin in the cyanobacterium *Synechococcus* sp. PCC 7002 causes a loss of photosystem I activity, J. Biol. Chem. 277 (2002) 20343–20354.

[51] W.C. Chan, P.D. White, Fmoc solid phase peptide synthesis: a practical approach, in: B.D. Hames (Ed.), The Practical Approach Series, Oxford University Press Inc., New York, USA, 2000.

[52] B. Guigliarelli, P. Bertrand, Application of EPR spectroscopy to the structural and functional study of iron–sulfur proteins, in: A.G. Sykes (Ed.), Advances in Inorganic Chemistry, Academic Press Inc., San Diego, USA, 1999, pp. 421–497.

[53] J.H. Golbeck, A comparative analysis of the spin state distribution of *in vivo* and *in vitro* mutants of PsaC a biochemical argument for the sequence of electron transfer as Fx→Fa→Fb, Photosyn. Res. 61 (1999) 107–144.

[54] M.L. Antonkine, C. Falzone, A. Hansen, F. Yang, J.H. Golbeck, Chemical rescue of site-modified ligands to the iron–sulfur clusters of PsaC in Photosystem I, in: G. Garab (Ed.), Photosynthesis: Mechanisms and Effects, Kluwer Academic publishers, The Netherlands, 1998, pp. 659–662.

[55] M.L. Antonkine, E.M. Maes, R.S. Czemuszewiez, C. Breitenstein, E. Bill, C.J. Falzone, R. Balasubramanian, C. Lubner, D.A. Bryant, J.H. Golbeck, Chemical rescue of a site-modified ligand to a 4Fe–4S cluster in PsaC, a bacterial-like dicluster ferredoxin bound to Photosystem I, Biochim. Biophys. Acta, Bioenerg. 1767 (2007) 712–724.

[56] L.A. Yu, I.R. Vassiliev, Y.S. Jung, D.A. Bryant, J.H. Golbeck, Modified ligands to F-A and F-B in photosystem I. 2. Characterization of a mixed ligand [4Fe–4S] cluster in the C51D mutant of PsaC upon rebinding to P700-F-X cores, J. Biol. Chem. 270 (1995) 28118–28125.

[57] T. Mehari, F.Y. Qiao, M.P. Scott, D.F. Nellis, J.D. Zhao, D.A. Bryant, J.H. Golbeck, Modified ligands to F-A and F-B in photosystem I. 1. Structural constraints for the formation of iron–sulfur clusters in free and rebound PsaC, J. Biol. Chem. 270 (1995) 28108–28117.

[58] H. Beinert, A.J. Thomson, 3-Iron clusters in iron–sulfur proteins, Arch. Biochem. Biophys. 222 (1983) 333–361.

[59] V. Schünemann, H. Winker, Structure and dynamics of biomolecules studied by Mössbauer spectroscopy, Rep. Prog. Phys. 63 (2000) 263–353.

[60] P. Middleton, D.P.E. Dickson, C.E. Johnson, J.D. Rush, Interpretation of Mossbauer spectra of 4-Iron ferredoxin from *Bacillus stearothermophilus*, Eur. J. Biochem. 88 (1978) 135–141.

[61] J.T. Hoggins, H. Steinfink, Empirical bonding relationships in metal-iron-sulfide compounds, Inorg. Chem. 15 (1976) 1682–1685.

[62] P. Hofer, A. Grupp, H. Nebenfuhr, M. Mehring, Hyperfine sublevel correlation (Hyscore) spectroscopy — a 2d electron-spin-resonance investigation of the squaric acid radical, Chem. Phys. Lett. 132 (1986) 279–282.

[63] B.A.C. Ackrell, E.B. Kearney, W.B. Mims, J. Peisach, H. Beinert, Iron–sulfur cluster-3 of beef heart succinate-ubiquinone oxidoreductase is a 3-iron cluster, J. Biol. Chem. 259 (1984) 4015–4018.

[64] R. Cammack, A. Chapman, J. McCracken, J. Peisach, Electron spin-echo spectroscopy of the iron–sulfur clusters of xanthine-oxidase from milk, J. Chem. Soc., Faraday Trans. 87 (1991) 3203–3206.

[65] R. Cammack, A. Chapman, J. McCracken, J.B. Cornelius, J. Peisach, J.H. Weiner, Electron spin-echo spectroscopic studies of *Escherichia coli* fumarate reductase, Biochim. Biophys. Acta 956 (1988) 307–312.

[66] J.K. Shergill, R. Cammack, J.H. Weiner, Electron spin-echo envelope modulation and spin–spin interaction studies of the iron–sulfur clusters in fumarate reductase of *Escherichia coli*, J. Chem. Soc., Faraday Trans. 87 (1991) 3199–3202.

[67] R. Cammack, K.L. Kovacs, J. McCracken, J. Peisach, Spectroscopic characterization of the nickel and iron–sulfur clusters of hydrogenase from the purple photosynthetic bacterium *Thiocapsa roseopersicina*. 2. Electron spin-echo spectroscopy, Eur. J. Biochem. 182 (1989) 363–366.

[68] S.A. Dikanov, M.K. Bowman, Determination of ligand conformation in reduced [2Fe–2S] ferredoxin from cysteine beta-proton hyperfine couplings, J. Biol. Inorg. Chem. 3 (1998) 18–29.

[69] A. Houseman, B. Oh, M. Kennedy, C. Fan, M. Werst, H. Beinert, J. Markley, B. Hoffman, N-14, N-15, C-13, Fe-57 and H-1, H-2 Q-band ENDOR study of Fe–S proteins with clusters that have endogenous sulfur ligands, Biochemistry 31 (1992) 2073–2080.

[70] P.E. Doan, C. Fan, B.M. Hoffman, Pulsed ^{1,2}H ENDOR and ^{2}H–^{2}H TRIPLE resonance of H-bonds and cysteinyl beta-CH_2 of the *D. gigas* hydrogenase $[3Fe–4S]^+$ cluster, J. Am. Chem. Soc. 116 (1994) 1033–1041.

[71] D.T. Edmonds, P.A. Speight, Nitrogen quadrupole resonance in amino acids, Phys. Lett. 34A (1971) 325–326.

[72] R. Blinc, M. Mali, R. Osredkar, J. Seliger, L. Ehrenber, N-14 Quadrupole-resonance in polyglycine, Chem. Phys. Lett. 28 (1974) 158–159.

[73] F. Lendzian, J. Rautter, H. Kass, A. Gardiner, W. Lubitz, ENDOR and pulsed EPR studies of photosynthetic reaction centers: protein–cofactor interactions, Phys. Chem. Chem. Phys. 100 (1996) 2036–2040.

[74] A.T. Gardiner, S.G. Zech, F. MacMillan, H. Kass, R. Bittl, E. Schlodder, F. Lendzian, W. Lubitz, Electron paramagnetic resonance studies of zinc-substituted reaction centers from *Rhodopseudomonas viridis*, Biochemistry 38 (1999) 11773–11787.

[75] W. Lubitz, G. Feher, The primary and secondary accepters in bacterial photosynthesis III. Characterization of the quinone radicals $Q_A^-\cdot$ and $Q_B^-\cdot$ by EPR and ENDOR, Appl. Magn. Res. 17 (1999) 1–48.

[76] K. Mukai, T. Kimura, J. Helbert, L. Kevan, Environment of iron–sulfur chromophore in adrenodoxin studied by EPR and ENDOR spectroscopy, Biochim. Biophys. Acta 295 (1973) 49–56.

[77] R. Kappl, M. Ebelshauser, F. Hannemann, R. Bernhardt, J. Huttermann, Probing electronic and structural properties of the reduced 2Fe–2S cluster by orientation-selective H-1 ENDOR spectroscopy: Adrenodoxin versus Rieske iron–sulfur protein, Appl. Magn. Res. 30 (2006) 427–459.

[78] M. Flores, R. Isaacson, E. Abresch, R. Calvo, W. Lubitz, G. Feher, Protein–cofactor interactions in bacterial reaction centers from *Rhodobacter sphaeroides* R-26: II. Geometry of the hydrogen bonds to the primary quinone Q_A^- by H-1 and H-2 ENDOR spectroscopy, Biophys. J. 92 (2007) 671–682.

[79] S. Sinnecker, M. Flores, W. Lubitz, Protein-cofactor interactions in bacterial reaction centers from *Rhodobacter sphaeroides* R-26: Effect of hydrogen bonding on the electronic and geometric structure of the primary quinone. A density functional theory study, Phys. Chem. Chem. Phys. 8 (2006) 5659–5670.

[80] A. Dey, E.J. Francis, M.W.W. Adams, E. Babini, Y. Takahashi, K. Fukuyama, K.O. Hodgson, B. Hedman, E.I. Solomon, Solvent tuning of electrochemical potentials in the active sites of HiPIP versus ferredoxin, Science 318 (2007) 1464–1468.

[81] J.H. Golbeck, K.G. Parrett, T. Mehari, K.L. Jones, J.J. Brand, Isolation of the intact photosystem I reaction center core containing P700 and iron–sulfur center F_X, FEBS Lett. 228 (1988) 268–272.

[82] K.G. Parrett, T. Mehari, P.G. Warren, J.H. Golbeck, Purification and properties of the intact P-700 and Fx-containing photosystem I core protein, Biochim. Biophys. Acta 973 (1989) 324–332.

[83] N. Li, P. Warren, J. Golbeck, G. Frank, H. Zuber, D. Bryant, Polypeptide composition of the photosystem I complex and the photosystem I core protein from *Synechococcus* sp. PCC 6301, Biochim. Biophys. Acta 1059 (1991) 215–225.

[84] K.G. Parrett, T. Mehari, J.H. Golbeck, Resolution and reconstitution of the cyanobacterial photosystem I complex, Biochim. Biophys. Acta 1015 (1990) 341–352.

[85] X.M. Gong, R. Agalarov, K. Brettel, C. Carmeli, Control of electron transport in photosystem I by the iron–sulfur cluster F_X in response to intra- and intersubunit interactions, J. Biol. Chem. 278 (2003) 19141–19150.

[86] Y.S. Jung, I.R. Vassiliev, F.Y. Qiao, F. Yang, D.A. Bryant, J.H. Golbeck, Modified ligands to F_A and F_B in photosystem I — Proposed chemical rescue of a [4Fe–4S] cluster with an external thiolate in alanine, glycine, and serine mutants of PsaC, J. Biol. Chem. 271 (1996) 31135–31144.

[87] L. Yu, D.A. Bryant, J.H. Golbeck, Evidence for a mixed-ligand [4Fe–4S] cluster in the C14D mutant of PsaC. Altered reduction potentials and EPR spectral properties of the F-A and F-B clusters on rebinding to the P700-F-x core, Biochemistry 34 (1995) 7861–7868.

[88] T. Hiyama, B. Ke, P430. Possible primary electron acceptor of photosystem I, Arch. Biochem. Biophys. 147 (1971) 99–108.
[89] T. Hiyama, B. Ke, New photosynthetic pigment, "P430": its possible role as the primary electron acceptor of photosystem I, Proc. Natl. Acad. Sci. U. S. A. 68 (1971) 1010–1013.
[90] K. Brettel, Electron transfer and arrangement of the redox cofactors in photosystem I, Biochim. Biophys. Acta, Bioenerg. 1318 (1997) 322–373.
[91] I.R. Vassiliev, Y.S. Jung, M.D. Mamedov, A.Y. Semenov, J.H. Golbeck, Near-IR absorbance changes and electrogenic reactions in the microsecond-to-second time domain in photosystem I, Biophys. J. 72 (1997) 301–315.
[92] P.V. Warren, J.H. Golbeck, J.T. Warden, Charge recombination between $P700^{+}$ and A_1^{-} occurs directly to the ground state of P700 in a photosystem I core devoid of F_X, F_B, and F_A, Biochemistry 32 (1993) 849–857.
[93] K. Brettel, J.H. Golbeck, Spectral and kinetic characterization of electron acceptor A_1 in a photosystem I core devoid of iron–sulfur centers F_X, F_B and F_A, Photosynth. Res. 45 (1995) 183–193.
[94] G.Z. Shen, M.L. Antonkine, A. van der Est, I.R. Vassiliev, K. Brettel, R. Bittl, S.G. Zech, J.D. Zhao, D. Stehlik, D.A. Bryant, J.H. Golbeck, Assembly of photosystem I: II. Rubredoxin is required for the in vivo assembly of F_X in *Synechococcus* sp. PCC 7002 as shown by optical and EPR spectroscopy, J. Biol. Chem. 277 (2002) 20355–20366.
[95] L.G. Rowan, E.L. Hahn, W.B. Mims, Electron spin echo envelope modulation, Phys. Rev. 137 (1965) A61–A71.
[96] S.A. Dikanov, Y.D. Tsvetkov, Electron Spin Echo Envelope Modulation (ESEEM) Spectroscopy, CRC Press, Boca Raton, Florida, USA, 1992.
[97] E.R. Davies, New pulse endor technique, Phys. Lett., A 47 (1974) 1–2.
[98] G. Feher, Observation of nuclear magnetic resonances *via* the electron spin resonance line, Phys. Rev. 103 (1956) 834–835.
[99] C. Calle, Pulse EPR methods for studying chemical and biological samples containing transition metals, Helv. Chim. Acta 89 (2006) 2495–2521.
[100] B.M. Hoffman, ENDOR of metalloenzymes, Acc. Chem. Res. 36 (2003) 522–529.
[101] W. Lubitz, E. Reijerse, M. van Gastel, NiFe and FeFe hydrogenases studied by advanced magnetic resonance techniques, Chem. Rev. 107 (2007) 4331–4365.
[102] W. Lubitz, F. Lendzian, R. Bittl, Radicals, radical pairs and triplet states in photosynthesis, Acc. Chem. Res. 35 (2002) 313–320.
[103] N.A. Stombaugh, J.E. Sundquist, R.H. Burris, W.H. Orme-Johnson, Oxidation–reduction properties of several low potential iron–sulfur proteins and of methylviologen, Biochemistry 15 (1976) 2633–2641.
[104] G. Battistuzzi, M. D'Onofrio, M. Borsari, M. Sola, A.L. Macedo, J.J.G. Moura, P. Rodrigues, Redox thermodynamics of low-potential iron–sulfur proteins, J. Biol. Inorg. Chem. 5 (2000) 748–760.
[105] J.P. Yu, L.B. Smart, Y.S. Jung, J. Golbeck, L. McIntosh, Absence of PsaC subunit allows assembly of photosystem I core but prevents the binding of PsaD and PsaE in *Synechocystis* sp. PCC 6803, Plant Mol. Biol. 29 (1995) 331–342.
[106] M. Ihara, H. Nishihara, K.S. Yoon, O. Lenz, B. Friedrich, H. Nakamoto, K. Kojima, D. Honma, T. Kamachi, I. Okura, Light-driven hydrogen production by a hybrid complex of a NiFe-hydrogenase and the cyanobacterial photosystem I, Photochem. Photobiol. 82 (2006) 676–682.